Tectonophysics 532–535 (2012) 134–155

Contents lists available at SciVerse ScienceDirect

Tectonophysics

journal homepage: www.elsevier.com/locate/tecto

Tectono-Sedimentary evolution and geochronology of the Middle Miocene Altınapa Basin, and implications for the Late Cenozoic uplift history of the Taurides, southern Turkey

Ayten Koç [a,*], Nuretdin Kaymakci [a], Douwe J.J. van Hinsbergen [b,c], Klaudia F. Kuiper [d], Reinoud L.M. Vissers [e]

[a] Department of Geological Engineering, Middle East Technical University, Ankara, 06531, Turkey
[b] Physics of Geological Processes, University of Oslo, Sem Sælands vei 24, NO-0316 Oslo, Norway
[c] Center for Advanced Study, Norwegian Academy of Science and Letters, Drammensveien 78, 0271 Oslo, Norway
[d] Department of Petrology, Free University of Amsterdam, De Boelelaan 1085, 1081 HV Amsterdam, The Netherlands
[e] Department of Earth Sciences, Utrecht University, 3508 TA Utrecht, The Netherlands

ARTICLE INFO

Article history:
Received 22 July 2011
Received in revised form 23 December 2011
Accepted 18 January 2012
Available online 1 February 2012

Keywords:
Miocene basins in Turkey
$^{40}Ar/^{39}Ar$ geochronology
Paleostress inversion
Eastern Mediterranean

ABSTRACT

The Tauride range in southern Turkey is flanked and overlain by Neogene sedimentary basins. To the south and on top of the high range, these basins are mainly marine, whereas poorly studied intramontane basins dominated by continental deposits are exposed to the north. In this paper, we study the stratigraphy and structure of the continental Altınapa Basin, and provide $^{40}Ar/^{39}Ar$ geochronology for volcanic deposits in the stratigraphy. The stratigraphy can be subdivided into a Lower Group, displaying ~400 m of fining upward fluvio-lacustrine sediments, unconformably overlain by an Upper Group with ~500 m of lacustrine deposits, andesitic lavas and volcaniclastic sediments. $^{40}Ar/^{39}Ar$ dating of three volcaniclastic samples across the Upper Group provide 11.8–11.6 Ma ages. The Altınapa Basin is an extensional basin, which formed predominantly due to N–S to NE–SW directed stretching. The main basin forming phase occurred during deposition of the Lower Group, prior to 11.8 Ma. Paleostress inversion analyses demonstrate uniaxial stress, with highly variable extension directions that are consistent with currently observed seismicity patterns. The Middle Miocene extension history of the Altınapa Basin is consistent with a regional pattern of Middle Miocene NE–SW to NW–SE extension north of the Cyprus subduction zone. This suggests that the Cyprus subduction zone has been in retreat relative to central Anatolia since at least Middle Miocene time. The continental Altınapa Basin is currently at an elevation of ~1 km, whereas partly contemporaneous marine sediments in the Mut Basin that lies on top of the Tauride range are elevated to 2 km. This shows strong late Cenozoic differential uplift in southern Turkey, with at least 1 km more uplift of the Tauride range than of the intramontane basins to the north. We conclude that the current high elevation of the Taurides is related to late Neogene extension and does not result from the late Cretaceous to perhaps Oligocene folding and thrusting that deformed the rocks in the range.

1. Introduction

In the eastern Mediterranean region (Fig. 1), convergence between Africa and Europe since the Cretaceous was accommodated by northward subduction of various branches of the Neotethys Ocean (Barrier and Vrielynck, 2008; Şengör and Yılmaz, 1981). As a result, the geology of Turkey includes a number of suture zones that demarcate the former positions of now subducted oceans. The most important of these is the İzmir–Ankara–Erzincan suture zone, where the Pontides to the north, belonging to Eurasia since the early Mesozoic (Torsvik and Cocks, 2009), and the Tauride–Anatolide Platform to the south, rifted away from Gondwana in the Triassic, collided after the complete subduction of the Northern Branch of the Neotethys. The collision of the Tauride–Anatolide Platform with the Pontides started at the end of Cretaceous and may have lasted until the end of the Eocene (Kaymakci et al., 2009; Meijers et al., 2010; Okay and Özgül, 1984; van Hinsbergen et al., 2010c). A second Cretaceous to Paleocene subduction zone existed to the south of the İzmir–Ankara suture zone, between the Kırşehir Block and the Taurides in central Turkey (the Inner Tauride Suture; e.g. Okay et al., 1996; Pourteau et al., 2010) and led to the formation of the Tauride fold–thrust belt in southern Turkey.

South of the Taurides, oceanic crust of the Southern Branch of the Neotethys still subducts today in the Cyprus subduction zone (Khair and Tsokas, 1999) (Fig. 1). In Eastern Turkey, this Southern Branch

* Corresponding author. Tel.: +90 3122105743.
E-mail address: kayten@metu.edu.tr (A. Koç).

0040-1951/$ – see front matter © 2012 Elsevier B.V. All rights reserved.
doi:10.1016/j.tecto.2012.01.028

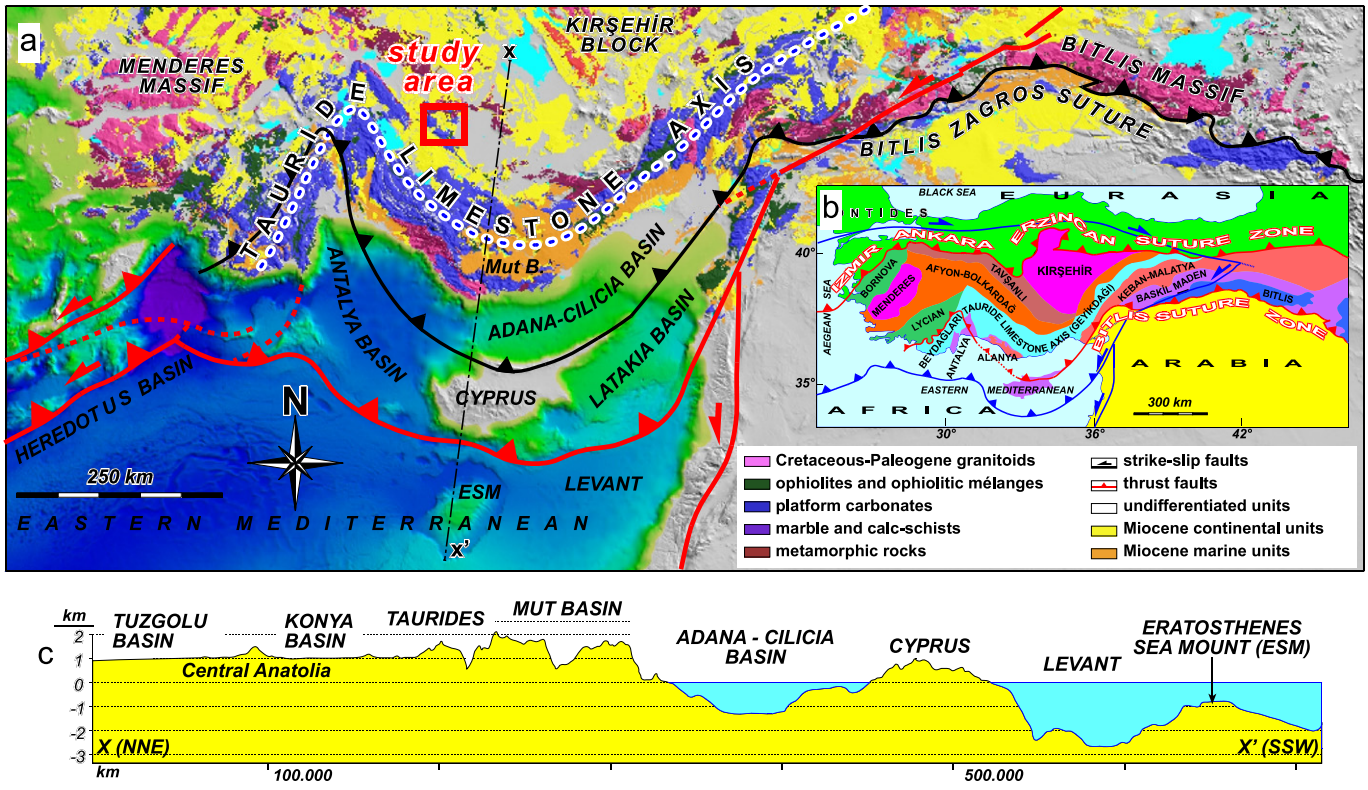

Fig. 1. a) Major tectonic zones of Turkey (modified from Okay et al. (1996) and Kaymakci et al. (2010). b) simplified geological map of southern Turkey overlaid on an SRTM topographic and bathymetric image (geological map is simplified from MTA 1/500.000 map series). c) Profile along the line XX′. Note that altitude of the Tauride range is ~1 km higher than the elevation of central Anatolia.

has been entirely subducted and is demarcated by the Bitlis suture zone, with the arrest of subduction at the end of the Middle Miocene (Faccenna et al., 2006; Hüsing et al., 2009; Keskin, 2003; Okay et al., 2010; Şengör and Yılmaz, 1981; Şengör et al., 2003). Subduction below the Taurides is in its latest stages, and was probably associated with slab break-off and slab roll-back processes since the Middle Miocene (Biryol et al., 2011; Faccenna et al., 2006; Gans et al., 2009; van Hinsbergen et al., 2010c).

The Tauride fold–thrust belt forms a carbonate-dominated mountain range in southern Turkey, with dominantly southward thrusting until Late Eocene time (Altıner et al., 1999; Andrew and Robertson, 2002; Mackintosh and Robertson, 2009; Meijers et al., 2011; Özer et al., 2004; Ricou et al., 1975). Although the belt shows large wavelength folds and thrusts, its high topography today is bounded by normal faults associated with Neogene sedimentary basins. These basins filled by marine to continental sediments and volcanics, formed in the overriding plate of the preset-day Cyprus subduction zone and their development may shed light on the geodynamic evolution of the eastern Mediterranean subduction zone since the Miocene. The dominantly marine basins are located mainly in the southern limb of the belt and include the well-described Adana, Mut and Antalya (including the Manavgat, Köprüçay and Aksu) basins (e.g. Bassant et al., 2005; Çiner et al., 2008; Darbas and Nazik, 2010; Derman and Gürbüz, 2007; Eriş et al., 2005; Gül, 2007; Janson et al., 2010; Karabıyıkoğlu et al., 2005; Poisson et al., 2003; Yetiş, 1988). A diachronous marine transgression flooded the southern part of the belt in Cyprus from the late Oligocene onward, and reached the Antalya, Mut and Adana regions in the north during the Early Miocene (Bassant et al., 2005).

To the north of the present-day Taurides, intramontane basins started to form during an ill-defined time interval in the Neogene. These include the Altınapa, Yalvaç and Ilgın basins (Fig. 2), descriptions of which are limited to Turkish language literature (Eren, 1993, 1996; Göğer and Kıral, 1969; Özcan et al., 1990; Özkan, 1998; Özkan and Söğüt, 1999; Yağmurlu, 1991a,b). The Altınapa Basin, located in the eastern limb of the Isparta Angle (Blumenthal, 1963) (Fig. 2), is one of the best exposed of these intramontane basins. It has a clastic and volcano-sedimentary infill of more than 850 m thick and rests on metamorphosed Mesozoic carbonates of the Tauride Belt, as well as on late high-pressure rocks of the inner-Tauride suture zone (Pourteau et al., 2010). These high-pressure rocks, with Cretaceous to Paleocene metamorphic ages, include Silurian–Permian meta-carbonates, flysch-type metaclastics and meta-magmatitic rocks (Karakaya, 1991), and massive Triassic–Cretaceous platform-type meta-carbonates, meta-dolerites and continental meta-clastics (Eren, 1996).

In this paper, the stratigraphic succession of the Altınapa Basin is described and $^{40}Ar/^{39}Ar$ geochronology from volcanics is provided.. In addition, we show results from kinematic studies aided by remote-sensing and field mapping techniques, and discuss the evolution of the basin in the context of the regional geodynamics and uplift of the Anatolian Plateau during the late Neogene.

2. Lithostratigraphy

The infill of the Altınapa Basin is dominated by continental clastic sediments, lava flows and volcaniclastic deposits. It was first mapped by Göğer and Kıral (1969), who included the entire Neogene stratigraphy in the Dilekçi Formation. After this pioneering study, various studies including Eren (1992, 1993, 1996), Özkan (1998), Özkan and Söğüt (1999), concentrated mainly on the Neogene stratigraphy. Eren (1993) made a detailed subdivision of the Neogene Dilekçi Formation into six lithostratigraphic units (Fig. 3). Özkan (1998) and Özkan and Söğüt (1999) provided additional stratigraphic data and introduced a revised stratigraphy and proposed five formations (Fig. 3). For the sake of convenience, we revise the lithostratigraphy

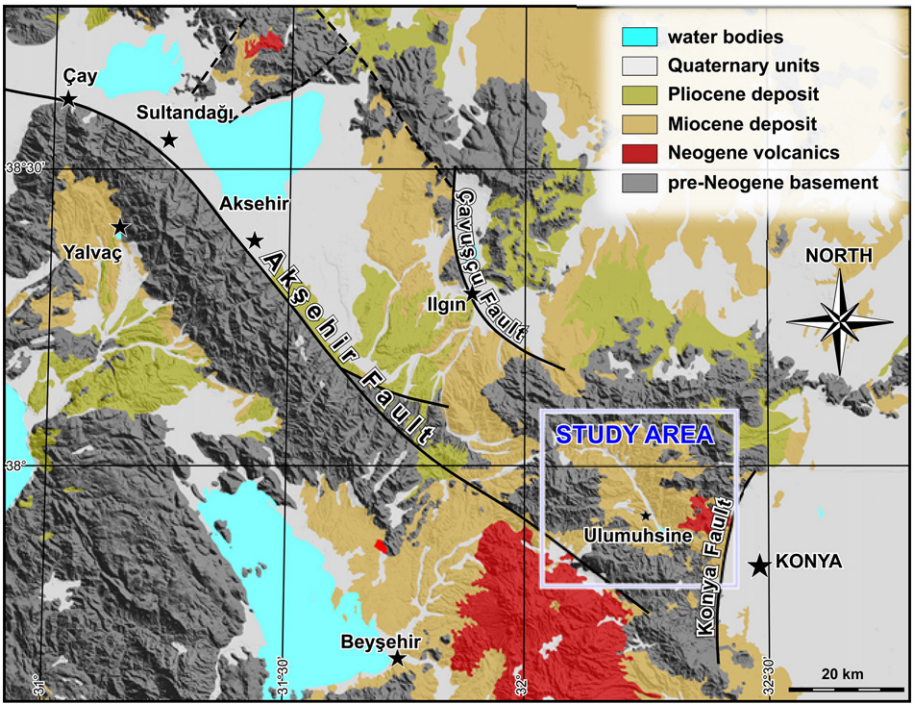

Fig. 2. Generalized geological map of the study area and its surrounding.

of the Neogene deposits in the Altınapa Basin and define three main stratigraphic units, namely the Lower and Upper Altınapa groups, and the Topraklı Formation, separated by regional unconformities. Below, we describe their lithology, age and contact relationships, and provide a first-order interpretation of their depositional environments (Fig. 4).

2.1. Lower Altınapa Group (LAG)

The LAG is characterized by conglomerate, sandstone and siltstone at the bottom, grading upwards and basinwards into claystone, marl, sandstone and medium to thick-bedded massive lacustrine limestones. These lithologies were included in the Dilekçi Formation by Göğer and Kıral (1969). Özkan and Söğüt (1999) divided this sequence into three separate formations, in which a lower conglomeratic unit is named "Sille Formation", an intermediate stromatolitic limestone unit "Yalitepe Formation" and an upper limestone/marl unit "Ulumuhsine Formation" (4). These units are well-exposed along the Kızılören Fault (Figs. 5 and 6a), near Dereaşıklar (Fig. 7) and north of Küçük Muhsine (Fig. 8) which was selected as the type locality for the LAG. It unconformably overlies Mesozoic basement, and is unconformably overlain by the Upper Altınapa Group.

The sequence starts at the bottom with coarse, angular, well-cemented, limestone-dominated breccias that grade upwards into reddish/purple, unsorted and polymict, subangular to subrounded pebble to boulder-size (occasionally up to 1 m diameter) conglomerates (Fig. 6b), overlying the high-relief carbonate basement of the Loras Mountain. At stratigraphically higher levels, sedimentary structures such as pebble imbrications and channel deposits are occasionally observed. The large clasts are dispersed in a poorly sorted, finer

Age			Niehoff, 1961 Konya,Ilgın	Wiesner, 1966 Sızma, Ladik	Göğer & Kıral, 1969 Kızılören	Görmüş, 1984 Kızılören	Özcan et al., 1988 Kutahya, Konya	Eren, 1993 Eldeş, Tepeköy	Özkan & Söğüt, 1999 Dilekçi, Konya	Revised Division	
QATERNARY			Alluviums	Alluviums	Alluviums	Alluviums		Alluviums	Alluviums	Alluviums	Alluv.
								Topraklı Formation	Topraklı Formation	Topraklı Formation Yürükler Formation	Topraklı Formation
CENOZOIC	Tertiary	Late Plio	Neogene Cover	Neogene Cover	Dilekçi Formation	Erenlerdağ Volcanics	Dilekçi Formation	Dilekçi Formation	Yürükler Formation K. Muhsine Formation Ulumuhsine Formation Yalıtepe Formation Sille Formation		
		Early Pliocene-Late Miocene								K. Muhsine Formation Ulumuhsine Formation	U. Altınapa Group
		Middle Miocene								Ulumuhsine Formation Yalıtepe Formation Sille Formation	L. Altınapa Group
		Early Miocene									

Fig. 3. Stratigraphic classification of the study area and its surroundings in previous studies, modified from Özkan (1998).

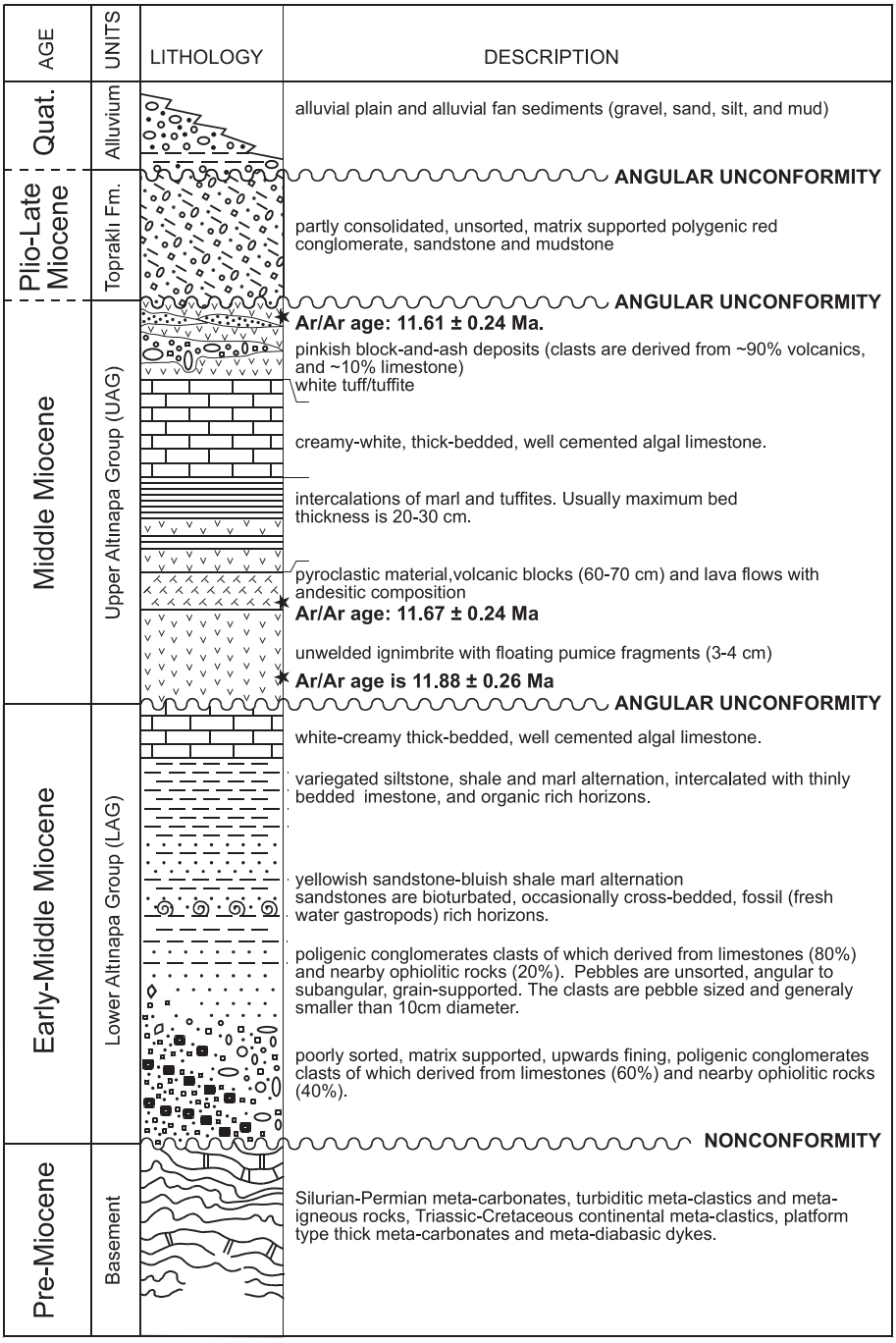

Fig. 4. Generalized stratigraphic column for the Altınapa Basin.

matrix and are typically matrix supported. These clasts consist mostly of sub-rounded limestones (60%) which have been deformed and contain calcite veins; subangular radiolarites, various radiolarian cherts and subrounded but ellipsoidal ultramafic rocks (~30%) dominated by serpentinites set in a silty–sandy matrix with ironoxide cement (Fig. 6c). The clast composition compares well with the regional basement lithology. The maximum observable thickness of this succession is approximately 200 m along the SW margin of the basin.

Around Dereaşıklar, the LAG turns to red, thick-bedded (Fig. 7), matrix supported (Fig. 6d) conglomerates, interfingering with dark gray to white, clast-supported, polymict conglomerates consisting of dominantly subangular to subrounded pebbles up to 10 cm diameter, with chert (20%) and limestone (80%) derived directly from the nearby basement (Fig. 6e). It unconformably overlies the basement, which consists of ophiolitic mélange (Fig. 7).

The location of the type section (Fig. 9) is chosen north of Küçük Muhsine village where, apart from the red basal conglomeratic unit, the complete sequence is exposed. In the type section, the sequence begins with conglomerates (Fig. 10a), which correspond to the dark gray to white, clast-supported, polymict conglomeratic unit in Dereaşıklar. The sequence continues upward with yellowish, occasionally cross-bedded and bioturbated, fresh-water gastropod bearing sandstones (Fig. 10b). It is succeeded towards the central and NE parts of the basin by rhythmic alternations of siltstone, green-blue coal bearing claystone, marls (Fig. 10d), and medium to thick (15 cm

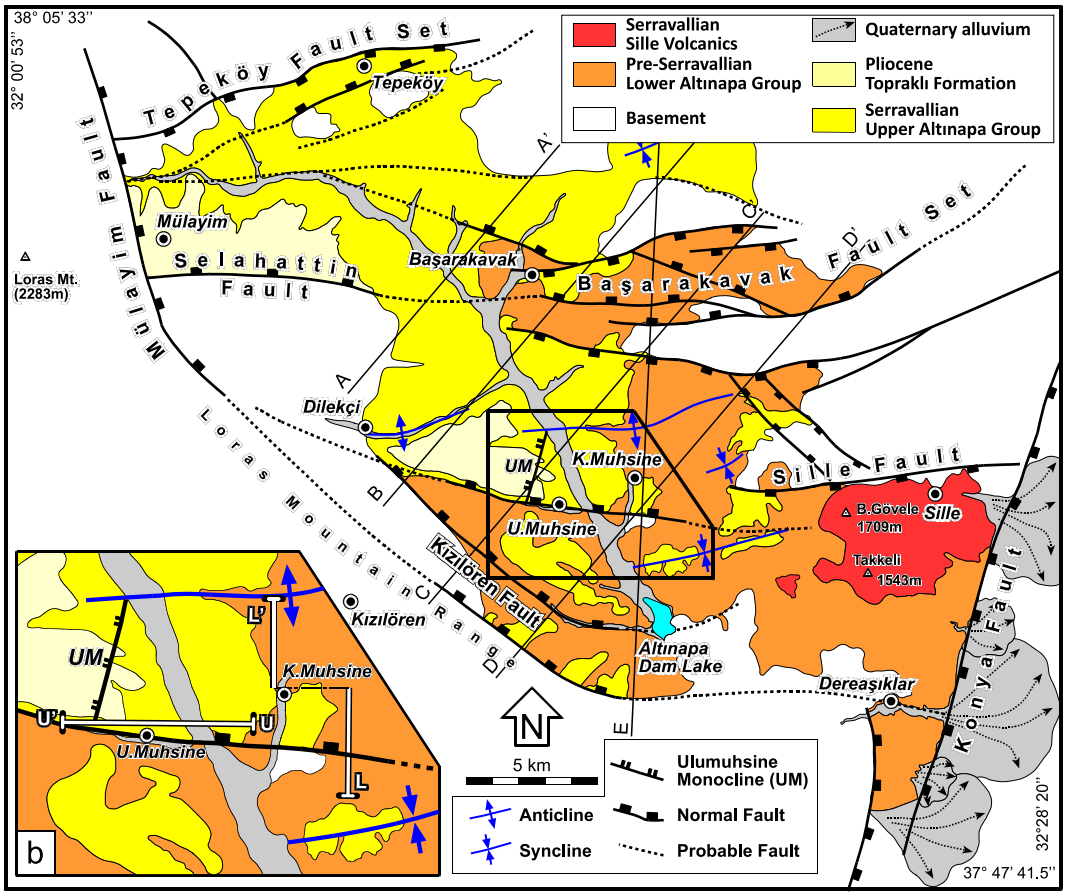

Fig. 5. (a) Revised geological map of the study area according to our mapping. (b) Inset map showing the location of the measured type sections for the Lower (L–L′) and Upper (U–U′) Altınapa groups. UM: Ulumuhsine Monocline. Dashed lines named as A, B, C, D and E indicate the trace of the cross-sections given in Fig. 20.

to 5 m) well bedded fresh water stromatolitic limestone (Fig. 10c). The LAG has a minimum thickness of 430 m.

From the Loras Mountain in the west to Küçük Mühsine village in the east, there is a gradual decrease in grain size from reddish conglomerates to fine grained yellowish/white marly deposits (Figs. 11 and 12). To the east of the Altınapa Lake near Küçük Muhsine Village, an erosional window provides exposure of the unconformity between the LAG and the underlying basement. The LAG in this area consists of much finer clastics than those adjacent to Loras Mountain. Similar grain size distributions are also observed elsewhere in the basin, and suggest that the basin detritus was dominantly shed from the SW margin. Note that the spatial distribution of the various lithologies as shown in Fig. 12 is consistent with that inference.

We did not observe fossils in the lower conglomeratic unit of the LAG, and previous studies (Eren, 1993; Özkan, 1998; Özkan and Söğüt, 1999) also did not report any fossil assemblages in this part of the LAG. To the west, however, around Kızılören, well outside of the Altınapa Basin, Görmüş (1984) reported fossil vertebrates including *Protoryx carolinae Major*, *Gazella deperdita Gaudry*, *Sus erymanthius Roth* and *Wagner*, *Prostrepticerus rothundicordis Weithofes*, *Ouis* sp. *Hiparious* sp., and *Ictitherium* sp. were collected from a red conglomeratic horizon pointing to Late Miocene–Pliocene age. Given the similar lithology, Özkan and Söğüt (1999) suggested a similar age for the LAG. We note, however, that the LAG underlies volcanics of the UAG, whereas the Kızılören overlies these. The age of the Kızılören unit therefore merely provides a minimum age for the LAG and UAG. On the other hand, Göğer and Kıral (1969) found fresh water fossils including *Unio* sp., *Radix* sp., ostracodes, bivalves and *Chara* sp. in limestones which have a lateral transition with these reddish conglomerates, and they suggested a Pliocene age. Eren (1993) assigned a Late Miocene–Early Pliocene age based on stratigraphic orders together with K/Ar radiometric ages obtained from the Konya volcanics to the east (Keller et al., 1977). Furthermore, Özkan (1998) described *Schizotrix* sp., *Chara* sp., and *Scytonema* sp. from their Yalitepe Formation, which corresponds to the central part of the LAG, and ascribed the formation to the Upper Miocene–Lower Pliocene. We note, however, that dating of endemic lacustrine fauna is subject to large uncertainties, and we will show that the age of the overlying Upper Altınapa Group is Middle Miocene based on our new $^{40}Ar/^{39}Ar$ data.

Unsorted, angular, occasionally reversely graded, matrix supported and boulder- to pebble-sized conglomerates indicate that the LAG was probably deposited in colluvial wedges, alluvial fans and terrestrial debris flows. From the SW margin towards the basin center, a gradual decrease occurs in the particles' size (Figs. 11 and 12), indicating a lateral transition from alluvial fans to lacustrine deposition. For the upper part of the LAG, lithologic characteristics (clay/siltstone and stromatolite limestone) and fossil content suggest a shallow lacustrine environment. Hence, the Lower Altınapa Group comprises facies associations extending from proximal alluvial fans along the basin margin to lacustrine facies in the central parts of the basin.

2.2. Upper Altınapa Group (UAG)

The UAG is characterized by limestones and marls interbedded with volcanic and volcaniclastic rocks. The limestone/marl and the volcano-sedimentary parts of the sequence have previously been subdivided into separate formations (Niehoff, 1961; Wiesner, 1968).

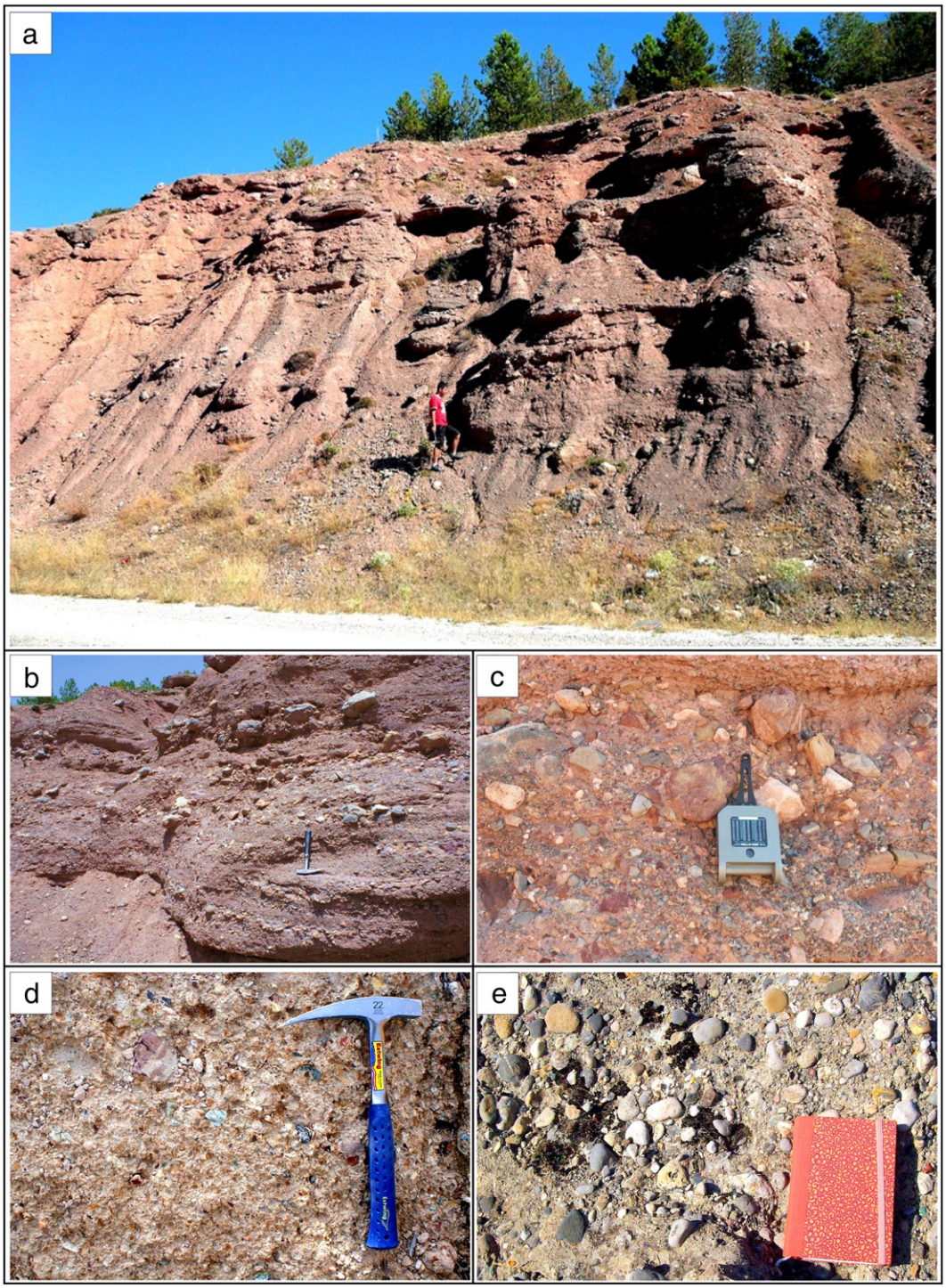

Fig. 6. Picture depicting basal conglomerates of the Lower Altınapa Group along the Kızılören Fault (a). Poorly bedded basal conglomerate observed along the Konya-Beyşehir Road (b). Close up view of the basal conglomerate with reverse graded beds (c). Note coarse, poorly sorted, subangular breccio-conglomerates. Matrix supported basal conglomerate, located close to Dereaşıklar (d). The conglomerate interfingeres with clast-supported, polymict conglomerates (e).

Göğer and Kıral (1969) included these rocks in the Dilekçi formation, in which the upper part of the sequence was named the Ulumuhsine limestone member, while the volcano-sedimentary parts were named the Küçük Muhsine Agglomerate Member and Erenkaya Tuff Member. On the other hand, Eren (1993) named the whole sequence, including limestone and volcanic rocks, Küçük Muhsine Formation (Fig. 3).

Around Küçük Muhsine (Figs. 8 and 12), the base of the UAG is defined by a well-exposed angular unconformity with the underlying LAG. To the north of Başarakavak, it onlaps onto basement rocks (Figs. 12 and 13). The UAG is unconformably covered by conglomerates of the Topraklı Formation (Fig. 14).

Unlike the LAG, the UAG contains intervals of volcanogenic material composed of intercalations of ignimbrites, dark gray to buff tuffs and tuffites, andesitic lava, lapilli/tuff and volcanic breccias (ash and block), intercalated with white to buff lacustrine limestones and creamy-white to greenish marls. These volcanic rocks are calc-alkaline in character and interpreted as belonging to the Miocene

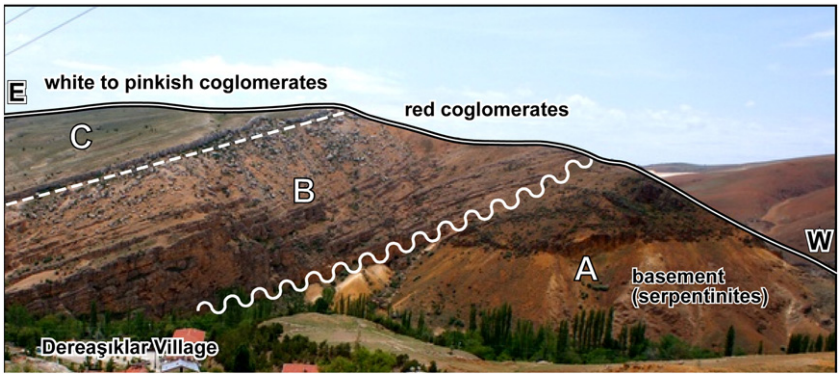

Fig. 7. Picture showing the basal conglomeratic unit of the Lower Altınapa Group near Dereaşıklar. Note the Neogene conglometatic unit unconformably overlies Mesozoic ophiolitic mélange. The white line is the Konya (normal) fault. View towards the East.

volcanic arc associated with the Cyprus subduction zone (Keller et al., 1977; Temel et al., 1998).

The type locality of the UAG starts from Küçükmühsine Village where the sequence starts with partly consolidated tuffs at the bottom (Fig. 15) and comprising floats of pumice fragments having diameters as large as 3–4 cm (Fig. 16a, b). The size and concentration of the pumice fragments increase upwards in each tuff horizon. The sequence continues upwards with a thick layer of volcanic breccia with andesite and dacite blocks with maximum block sizes up to 70 cm diameter. This level is succeeded by well-consolidated, well-bedded tuffite sequences with bed thicknesses up to 1 m and a total thickness of approximately 300 m. Tuffaceous layers generally contain crystals of plagioclase, quartz, biotite, amphibole, and volcanic glass (Eren, 1992). These sequences are succeeded by clay-marl alternations and intercalations of thick-bedded, well-cemented algal limestones. The thickness of the limestones around Ulumuhsine Village, where they are best exposed, is approximately 65 m (Figs. 14 and 15), while they are approximately 90 m around NE of Başarakavak Village located at north-eastern part of the study area. The top of the sequence consists of white tuff and tuffites and pinkish block-and-ash deposits (Figs. 14 and 16c, d). These deposits contain angular, poorly sorted clasts comprising 90% of volcanogenic and 10% of limestone origin. The sizes of the contained clasts are less than 30 and 10 cm, respectively. The measured stratigraphic thickness of the UAG is 480 m.

As mentioned above, Göğer and Kıral (1969) reported fresh water fossils in some limestone units, including *Unio* sp., *Radix* sp., *Planorbis* sp., ostracodes, and *Chara* sp. and suggested a Pliocene age for this formation. Özkan and Söğüt (1999) also proposed Late Miocene–early Pliocene age for the unit based on gastropoda fossils such as *Radix* sp., *Planorbis* sp., bivalves such as *Unio* sp., and algae such as *Chara* sp. These ages do not fit in our stratigraphy and radiometric ages. However, Alçiçek (2010) observed similar fossil assemblages together with some mammal fossils in SW Turkey which are indicating MN 3–4 Zone, an age range starting in the Burdigalian. Additionally, K–Ar ages of volcanic units in the east of the Altınapa Basin start as old as 11.95 Ma (Besang et al., 1977; Keller et al., 1977), which indicates the age of the volcanic activity in the Altınapa Basin and fits with our observations and age range. Therefore, the ages proposed by Göğer and Kıral (1969) and Özkan and Söğüt (1999) need to be revised.

The absence of conglomerates and channeled sandstones, as well as the dominance of clay/siltstone and limestone of the Upper Altınapa Group, and its fossil content indicate a quiet lacustrine environment, adjacent to volcanic centers.

2.3. Topraklı Formation

The Topraklı Formation unconformably covers the UAG (Fig. 14) and is characterized by reddish–brownish conglomerate, sandstone and occasional mudstone. It has a limited distribution close to the western boundaries of the basin (Fig. 12). The rocks were mapped as Topraklı conglomerates and Alluvium by Doğan (1975), and Eren (1993) and Özkan (1998) named the sequence "Topraklı Formation",

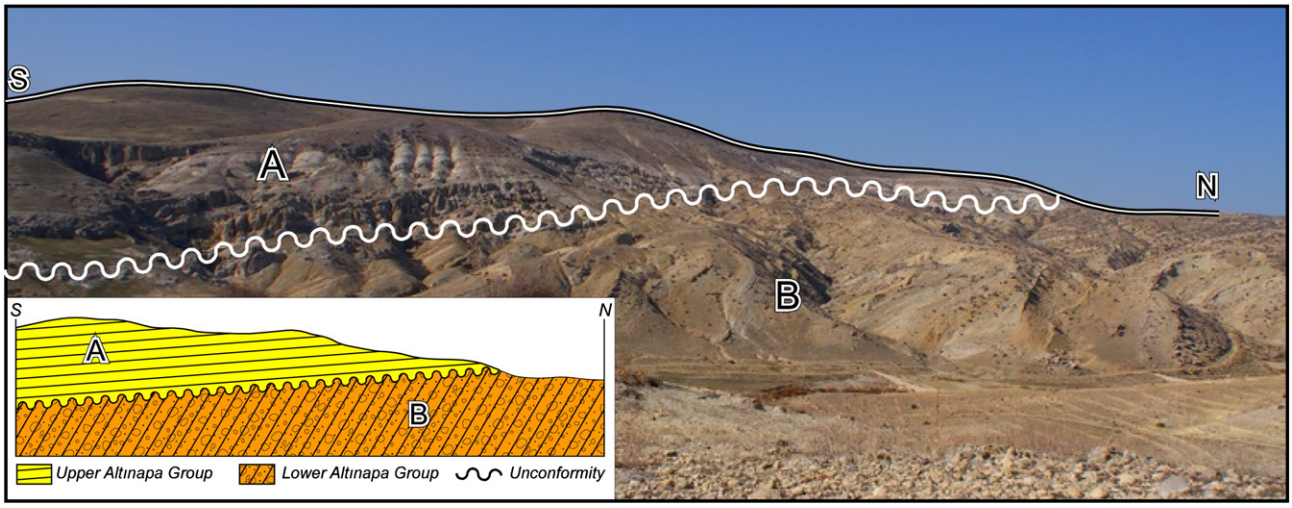

Fig. 8. Picture showing the angular unconformity between the Lower and Upper Altınapa groups.

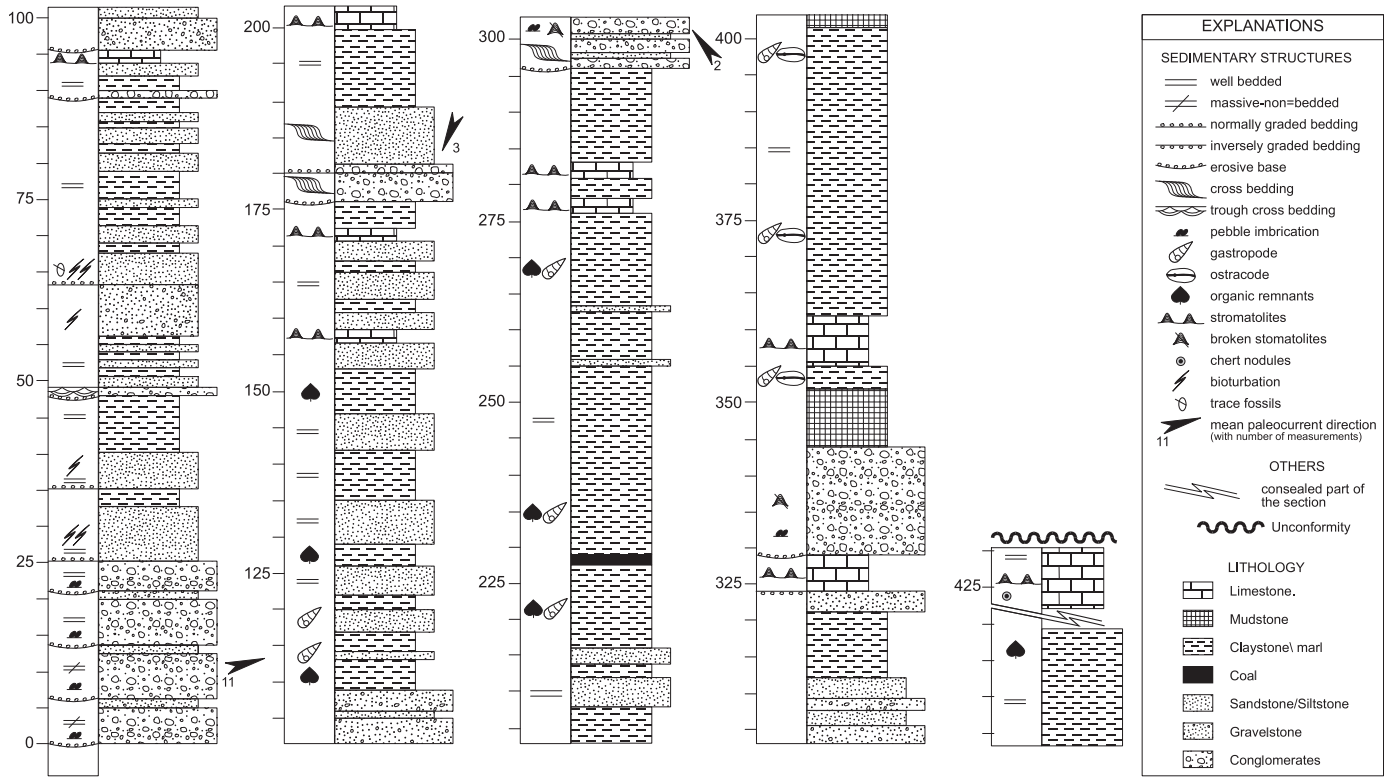

Fig. 9. Type-section of the Lower Altınapa Group.

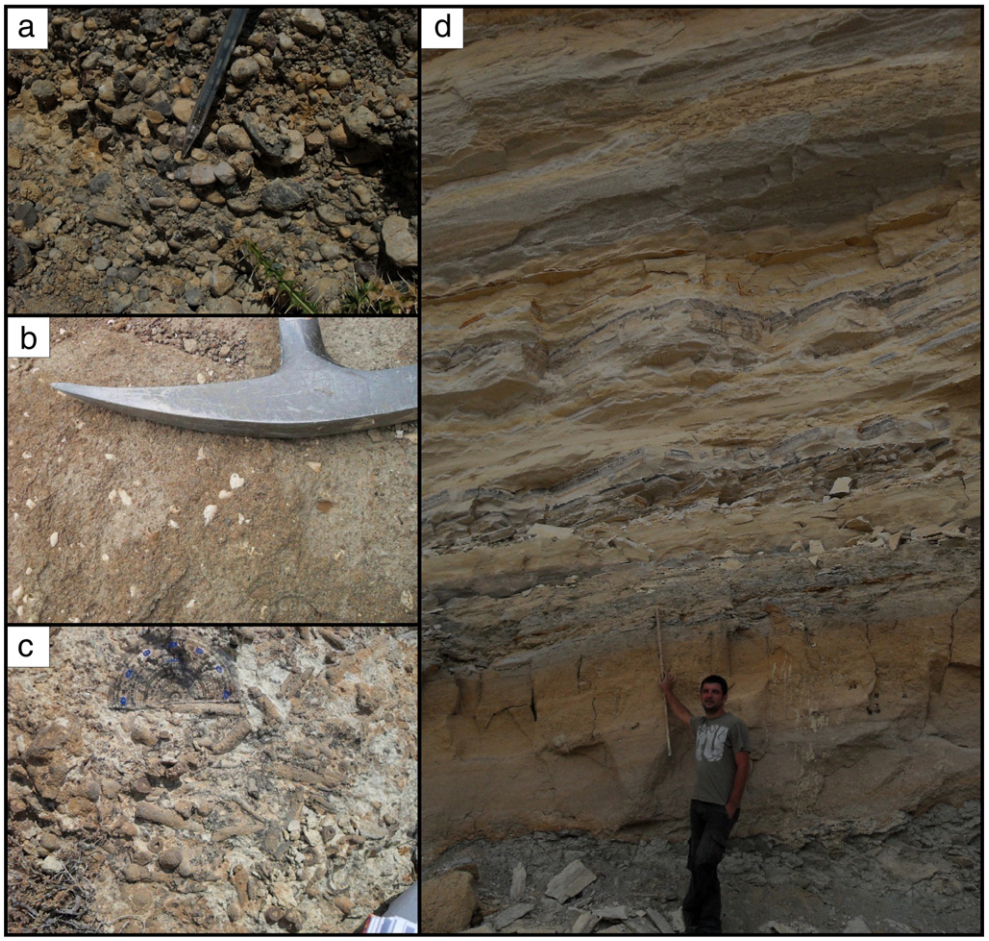

Fig. 10. Pictures showing typical facies of the Lower Altınapa Group: a) clast-supported, polymict conglomeratic units b) cross-bedded and bioturbated, fresh-water gastropods-bearing sandstones, c) well bedded fresh water stromatolitic limestone and d) alternation of siltstone, green-blue coal bearing claystone, marls.

Fig. 11. Picture depicting facies changes of Lower Altınapa Group from SW margin towards northeast into the basin center. The white line represents the Kızılören (normal) fault (ticks on the hanging-wall block). Note that coarse, poorly sorted, subangular coarse clastics dominate along the SW margin while they rapidly become finer-grained to marl-dominated towards NE (view to NW).

which is also adopted in this study. The Topraklı Formation is well exposed NW of the Ulumuhsine Village and it unconformably overlies pinkish tuffs and algal limestone belonging to the UAG (Figs. 12 and 14).

NW of Ulumuhsine, the formation is composed of a coarsening upward sequence of loosely cemented, unsorted and polymict, angular, pebble- to boulder-size (occasionally up to 80 cm diameter), matrix-supported conglomerates. Clasts originate from mostly limestones, sandstones, quartzites and cherts, i.e., lithologies that are abundant in the basement of the region. In addition, it reworks lacustrine limestone, dacite and andesite derived from Neogene units. The clasts are floating in a muddy/sandy matrix with iron-oxide cement. In addition, normally graded, polymict, sub-angular clast-supported conglomerates were also observed in some levels. Sedimentary structures such as planar cross-bedding and pebble imbrications are common in these stratigraphic levels. Another common facies within this unit comprises alternations of mudstone and matrix-supported conglomerate. There are also well-developed channels and occasional concretions within the mudstones, both indicating alluvial plain deposition with paleosol horizons.

No fossils have been observed from the unit, so far, and its age can only be constrained by superposition. The Topraklı Formation covers all of the Neogene units in the basin and is in turn overlain by Quaternary alluvium.

Unsorted, as well as upward-coarsening, matrix-supported and boulder- to pebble-size conglomerates with angular pebbles suggest

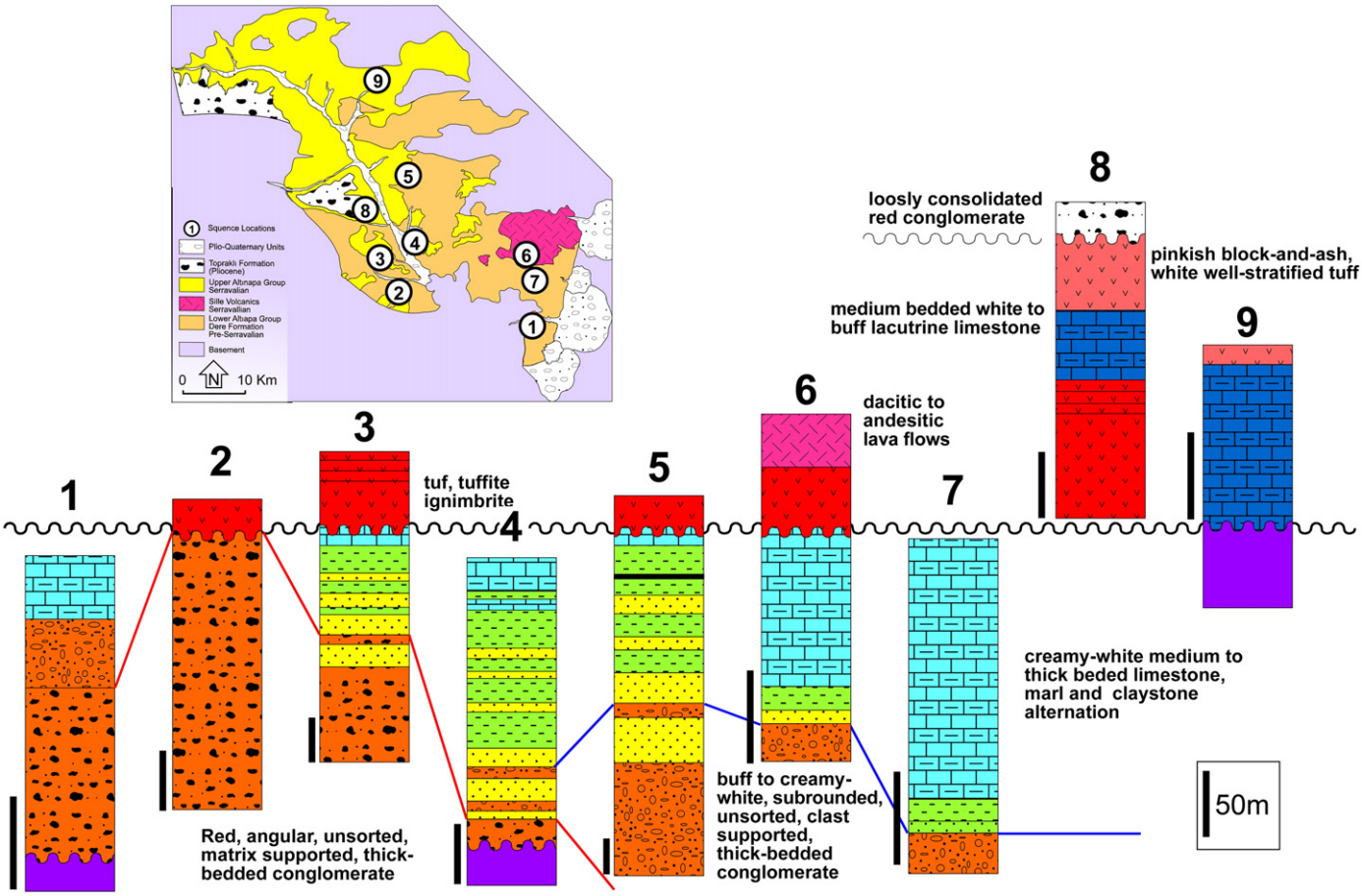

Fig. 12. Schematic illustration of the lithostratigraphy of the Altınapa Basin (not to scale). The section number is given on the geological map of the study area. Notice that grain size decreases from west to east. Vertical bars indicate the scales of each column independently.

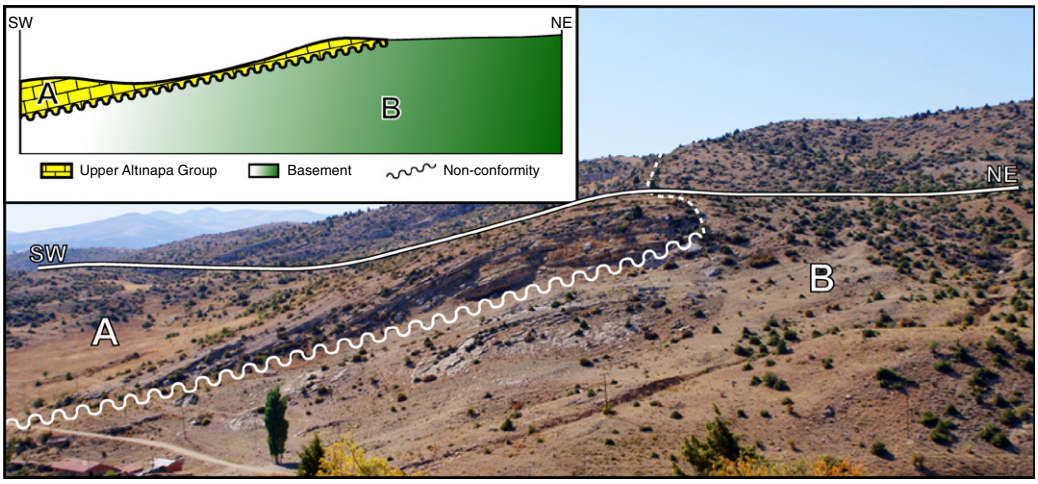

Fig. 13. Picture showing onlapping lacustrine algal limestones of the Upper Altınapa Group over the basement (location is 2 km north of Başarakavak, view to NW).

deposition in alluvial fans and continental debris flows. Additionally, sub-rounded, normally graded, grain-supported conglomerates showing pebble imbrications and erosional surfaces represent channeled fluvial stages within the alluvial fan deposition. Mudstones were most likely deposited by over concentrated currents, which define the flooding area and the distal part of the alluvial fan deposits. The caliche profiles in the mudstone suggest interruptions of sedimentation in a dry environment.

3. $^{40}Ar/^{39}Ar$ geochronology

Because previous age assignments rely on poorly dated endemic lacustrine faunae, we provide three $^{40}Ar/^{39}Ar$ ages from lavas and pumice horizons in the UAG (Fig. 4). One sample was taken from the lowermost lava we encountered (S3), one sample was taken from a gray tuff halfway the sequence (S2), and the third was collected from the uppermost pinkish tuffs (S1).

Bulk samples were crushed, washed and sieved. Grain size fractions of 1000–2000 μm (S1, S2) or 500–1000 μm (S3) were used for standard magnetic and heavy liquid separations. Final mineral fractions were separated by hand-picking under a microscope. The samples were wrapped in Al-foil packages and loaded in a 9 mm ID quartz vial. Between each set of 4 samples and at top and bottom positions, Fish Canyon Tuff sanidine (FCs) standard was used as neutron fluence monitor. The vial was irradiated for 10 h in the OSU Triga CLICIT facility, USA. After irradiation, samples and standards were loaded in 2 mm diameter holes of a copper tray and placed in an ultra-high vacuum extraction line. Single crystal $^{40}Ar/^{39}Ar$ fusion experiments were performed at the Vrije Universiteit Amsterdam, The Netherlands using a Synrad 48–5 CO_2 laser and custom made beam delivery system. Samples were purified in an in-house designed sample clean up line and analyzed on a MAP215-50 noble gas mass spectrometer fitted with a Balzers SEV217 detector. Mass discrimination was monitored by 3 replicate runs of air pipettes every 12 unknowns and blanks were run every 3 unknowns.

Ages are calculated using the in-house developed ArArCalc software (Koppers, 2002) with Steiger and Jäger (1977) decay constants. Ages are calculated relative to the FCs of 28.198 ± 0.23 Ma (Kuiper et al., 2008); note that this study reports 28.201 Ma using decay constants of Min et al. (2000), which converts to 28.198 Ma using Steiger and Jäger (1977). Correction factors for neutron interference reactions are $(2.64 \pm 0.04) \times 10^{-4}$ for $(^{36}Ar/^{37}Ar)_{Ca}$, $(6.73 \pm 0.08) \times 10^{-4}$ for $(^{39}Ar/^{37}Ar)_{Ca}$, $(1.211 \pm 0.006) \times 10^{-2}$ for $(^{38}Ar/^{39}Ar)_{K}$ and $(8.6 \pm 1.4) \times 10^{-4}$ for $(^{40}Ar/^{39}Ar)_{K}$. The $^{40}Ar/^{36}Ar$ ratio of 295.5 of Nier (1950) is used in the calculations. Errors are reported at 2 sigma level. Outliers are identified by comparing MSWD with the T-student distributions. The summary of the $^{40}Ar/^{39}Ar$ results is given Table 1 and plateaus and isochrones are given in Fig. 17. Full analytical data are given in the Supplementary Data.

Sample S2 is the deepest level in the statigraphy (Fig. 4). It does not yield a reliable weighted mean age. The sample is low on potassium and has low radiogenic ^{40}Ar yields. It most likely represents a glass fraction. The inverse isochron shows clear indications of excess argon and the inverse isochron age is 11.88 ± 0.11 Ma (± 0.26 Ma, full external error). K and/or Ar mobility can be an issue in glass fractions (Morgan et al., 2009) and this age is therefore considered to be

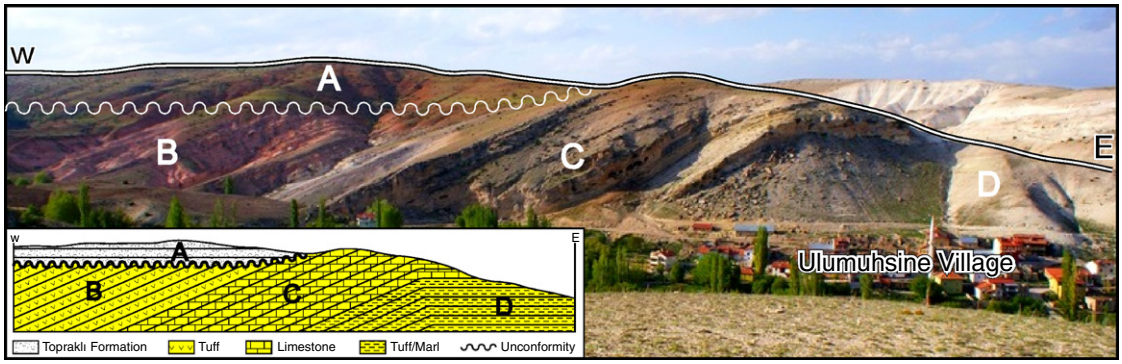

Fig. 14. Picture showing the angular unconformity between the Upper Altınapa Group (UAG) and overlying Topraklı formation near Ulumuhsine. The UAG consists of pinkish/white tuff, freshwater limestone (65 m) and marl/tuff alternation.

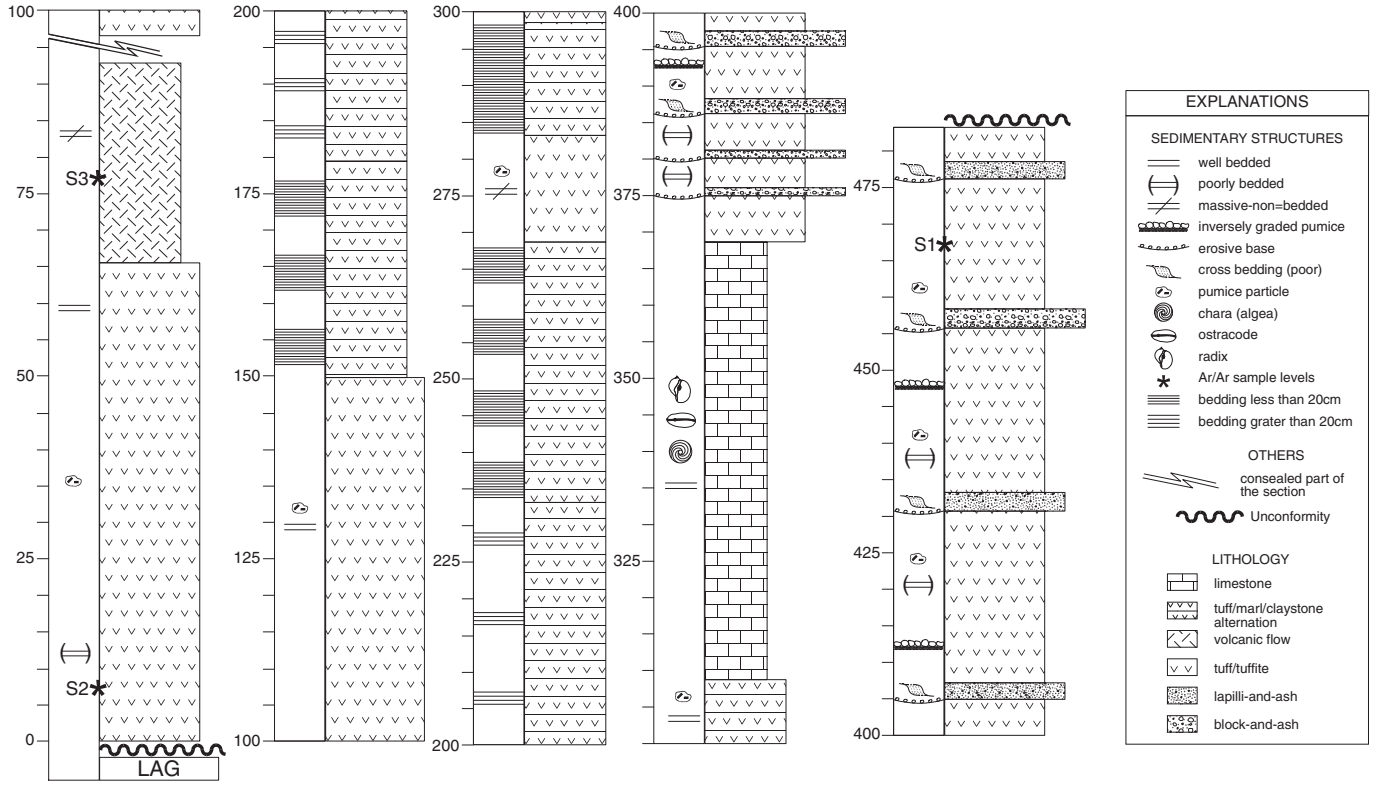

Fig. 15. Type-section of the Upper Altınapa Group around Ulumuhsine (see Fig. 5b for location of the section).

less reliable. However, its age is consistent with the stratigraphy with samples S3 and S1 being younger and stratigraphically higher in the section.

Sample S3 has a mixed population of grains based on K/Ca ratios. The four youngest grains with highest K/Ca ratio yield a weighted mean age of 11.67 ± 0.05 Ma (± 0.24 Ma full external error).

Sanidine of the highest sample S1 yields a weighted mean age of 11.61 ± 0.02 Ma (analytical error); or ± 0.24 Ma (full external error including standard age and decay constant uncertainties). The sample has high radiogenic $^{40}Ar^{*}$ contents and therefore data points cluster together on the isochrones. Although the $^{40}Ar/^{36}Ar$ atmospheric intercept on the inverse isochron deviates from the atmospheric intercept the weighted mean and isochron ages are similar.

4. Structural geology

The major structures which shaped the Altınapa Basin include large scale normal faults, numerous mesoscopic faults commonly with no more than a few meters offset, and non-systematic open folds. Most of these structures were mapped using remote sensing techniques and subsequently verified in the field. Kinematic data were collected from mesoscopic faults for construction of paleostress configurations.

4.1. Remote sensing

The applied remote sensing techniques include processing and interpretation of satellite images and interpretation of stereographic aerial photographs of 1/40.000 scale, using mirror stereoscopes. The used satellite imagery includes Landsat TM and ETM^{+}and Terra-ASTER images. In addition, Quickbird images obtained from Google Earth were used for areas where higher resolution was required. All of these images were co-registered using 1/25.000 scale topographical maps and combined in a GIS medium together with previously obtained maps and a field database.

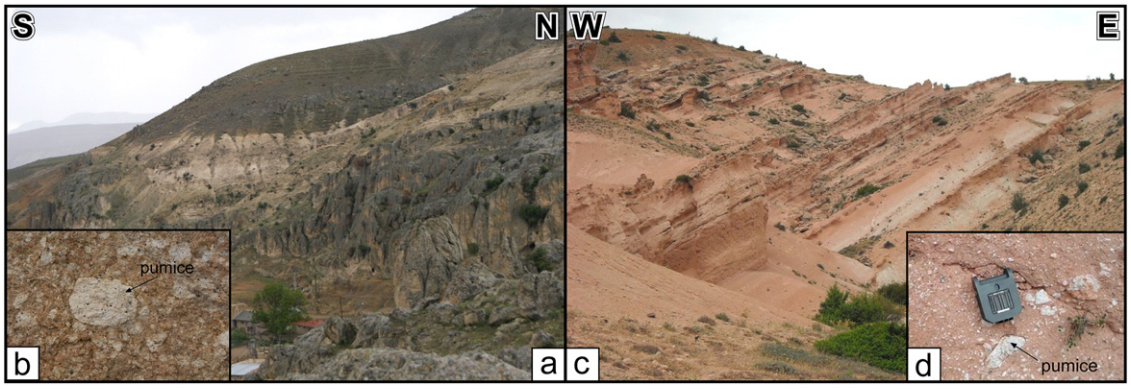

Fig. 16. Tuff facies of Upper Altınapa Group (UAG). a) The tuff facies at the bottom andb) their close up view. c) block and ash facies at the top of the UAG and d) their close up view.

Table 1
Summary of $^{40}Ar/^{39}Ar$ data. Full data tables are given in the appendix. Errors are reported with 2σ uncertainty and represent analytical error. Full external errors are reported between brackets. MWSD is Mean Square Weighted Deviate. N is the number of analysis included in the weighted mean age, between brackets the number of experiments excluded.

Irradiation ID	Location		Material	Weighted mean age	MSWD	N	Inverse ısochron	$^{40}Ar/^{36}Ar$ ıntercept
	Long	Lat						
VU78B-S1	32.24106	37.92545	Sanidine	11.54 ± 0.02(0.24)	1.61	9(1)	11.53 ± 0.01(0.24)	333 ± 25
VU78B-S2	32.28291	37.92859	Glass	No reliable age	0.48	7(3)	11.88 ± 0.11(0.26)	310.6 ± 2.3
VU78B-S3	32.26722	37.92645	Feldspar	11.67 ± 0.05(0.24)	1.14	4(5)	11.70 ± 0.03(0.24)	276 ± 11

In addition to aerial photos and satellite images, 25 x 25 m resolution digital elevation models (DEMs) prepared from 1/25.000 scale topographical maps were used, together with 90 x 90 m (3 arc sec) resolution Shuttle Radar Topographical Mission (SRTM) data. These images and DEMs have different spatial resolutions, which is useful for detection and delineation of structures at different scales. In addition, the images were draped on the DEMs for 3D visualization in different directions, enhancing morphological expressions of structures in all directions. After the images were enhanced, lineaments were delineated manually on the images. Lineaments showing appreciable morphological expressions were labeled as faults. Digital elevation data and a resultant lineament map are shown in Fig. 18. In addition, a length-weighted rose diagram prepared from the trends of these structures (Fig. 18) displays two dominant directions (NE–SW and NW–SE) having approximately 60° acute angles.

4.2. Field observations

The major structures that shaped the Altınapa Basin are normal faults along at the margins of the basin. The basin stratigraphy is deformed along gentle to open folds and, in one locality, in a conspicuous 100 m scale monocline. In addition, numerous mesoscopic faults, which developed after and during sedimentation (Fig. 19) have pervasively affected the basin (Fig. 5).

Morphologically, the most prominent faults are identified at the margins of the basin (Fig. 5). Generally they are recognized as linear to curvilinear mountain fronts rising steeply at the contact of the basin fill units and basement rocks. Among these, the Kızılören Fault (KF) is inferred mainly on the basis of a thick accumulation of red clastics abutting against the basement rocks, although the main fault plane was not observed during field studies (Fig. 5). Nevertheless, the fault zone is characterized by smaller scale syn- and antithetic normal faults exposed along the sediment-basement contact.

The Mülayim Fault (MF) is oriented NNW–SSE and dips to the NE. It controls the northwestern margin of the basin and separates gently dipping Plio-Quaternary Topraklı sediments from the carbonate basement units (Fig. 18). Along the fault, the basin fill units are characterized by unsorted, angular to sub-angular, boulder- to pebble-size (up to 1 m) sedimentary breccias and conglomerates. In Mülayim village, adjacent to the fault, the basin fill units are almost horizontal.

The Tepeköy Fault Set (TFS) located at the northern margin of the basin comprises two ENE–WSW oriented conjugate normal faults. The northern branch of the fault set dips southwards while the southern branch dips northwards defining a graben around Tepeköy (Fig. 5). Both of the branches of the TFS extend beyond the present boundaries of the Altınapa Basin and are delimited in the SW by the Mülayim Fault, which is almost perpendicular to the TFS. The south-dipping branch of the Tepeköy Fault delimits the northern boundary of the basin. The basement at this part of the basin comprises Paleozoic to Jurassic marbles and quartzites.

The Selahattin Fault (SF) is developed in the NW part of the study area and is oriented parallel to the TFS. It is also delimited by the Mülayim Fault in the west. Along the SF the Topraklı Formation is juxtaposed with the basement units, which are composed mainly of Triassic carbonates. The eastward continuation of the fault within the Upper Altınapa Group is uncertain. Morphologically, however, the fault can be followed eastward where it seems to link-up with one of the north-dipping branches of Başarakavak Fault Set (BFS) (Fig. 5).

The Başarakavak Fault Set (BFS) comprises a number of E–W striking faults with horst and graben morphology. Along the major faults of the BFS, basement and basin fill units are juxtaposed. Lateral continuity of the fault set within the basement is morphologically well expressed while within the basin towards the west the BFS is not exposed.

The southeastern boundary of the basin is delineated by the active (Öğütcü et al., 2010) Konya Fault which controls the northwestern boundary of the vast Konya Plain. The Konya fault is about 45 km long and shows an approximately NNE–SSW trend. It dips SE and separates the Neogene sedimentary fill of the Altınapa Basin in the footwall from the Quaternary alluvial sediments of the Konya Basin in the hanging wall. Well preserved fault planes with slip lines are exposed, and linear coalesced alluvial fan and apron systems developed within the Konya Basin, consistent with its ongoing activity as evident from the 11 September 2009 Sille Earthquake, (Mw = 4.9) along the fault. Finally, the eastern margin of the basin is characterized by onlap of lacustrine algal limestones of the UAG (Figs. 13 and 20), showing an asymmetric development of the basin.

The mainly E–W trending open folds that deform the stratigraphy of the Altınapa Basin are developed within both the Lower and Upper Altınapa groups. However, the dips of the limbs of these folds seem more gentle within the Upper Altınapa Group, with dips not exceeding 30°, whereas they are steeper within the Lower Altınapa Group, with dips up to 50° (Fig. 20). All of these folds form a series of anticlines and synclines parallel to the Tepeköy and Başarakavak Faults and almost perpendicular to the NNW–SSE trending basin bounding faults (Kızılören Fault). Their maximum observed wavelength is approximately 10 km and they developed in the hanging-walls of the normal faults. An exception to this general fold trend is formed by the Ulumuhsine Monocline, which strikes N15E, parallel to the Konya Fault and dips 30° W (Figs. 5, 14 and 20). This monocline, which is consistent with a buried blind normal fault at depth, deforms the UAG, but is unconformably covered by the Topraklı Formation.

5. Paleostress analysis

5.1. Data and method

In addition to the large-scale structural analysis, we carried out a detailed kinematic analysis from mesoscopic structures in order to unravel paleostress configurations during the development of the Altınapa Basin.

The paleostress configurations are reconstructed using Angelier's software to analyse fault slip data collected from exposed fault planes. Analysis of fault attitudes and their associated directions and sense of slip are used to infer principal stresses, a procedure also known as paleostress inversion (Angelier, 1990; 1994; Carey and Burinier, 1974; Etchecopar et al., 1981). Two assumptions are fundamental to these methods: 1) the bulk state of stress in a small area is uniform, and 2) the slip direction is parallel to the maximum resolved shear

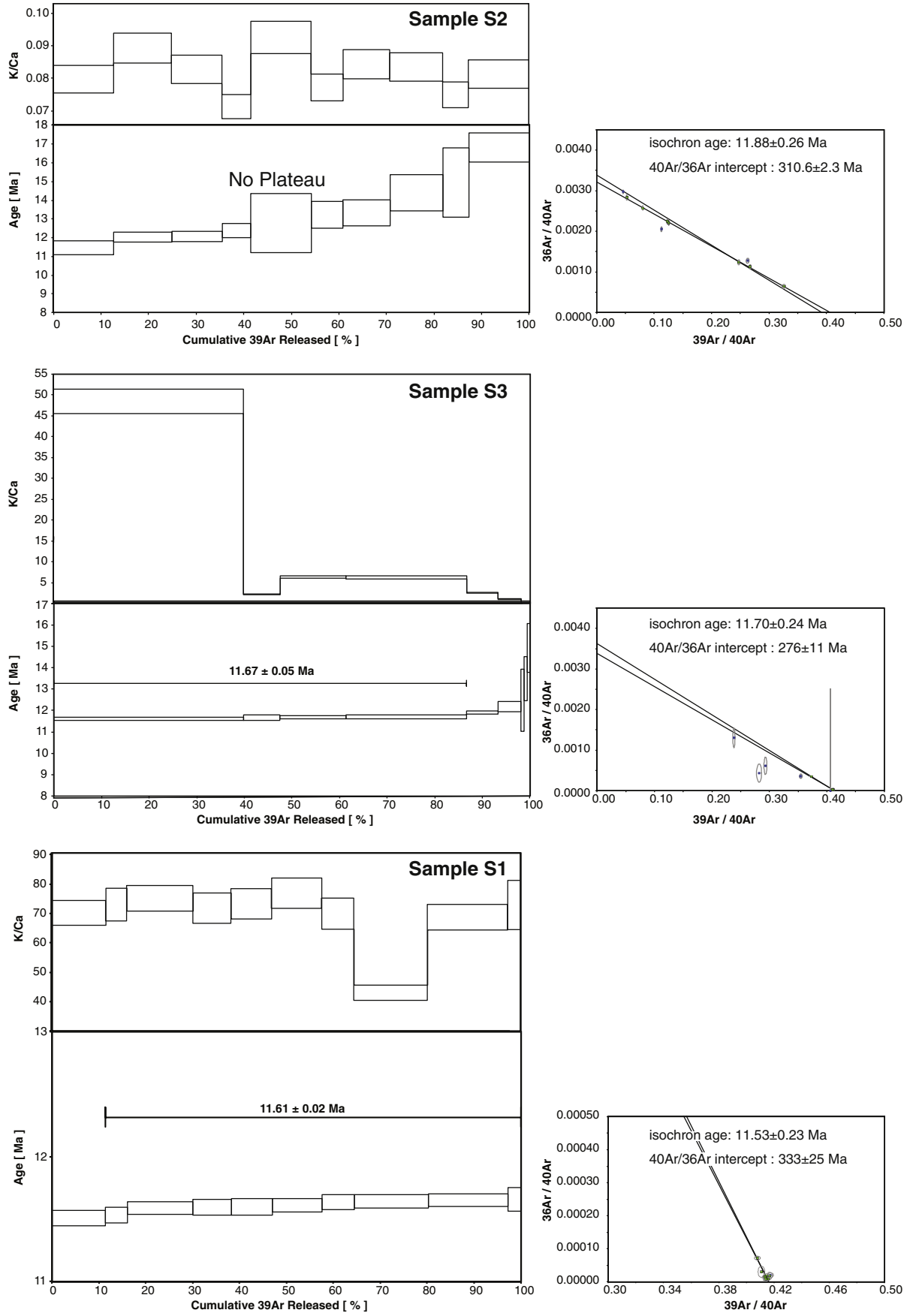

Fig. 17. Replicate single crystal fusion $^{40}Ar/^{39}Ar$ ages are plotted versus the% of ^{39}ArK released in each fusion analysis for the three lava samples from the Upper Altınapa Group. The width of the bars/steps represents the 2σ analytical error. On top the K/Ca ratio (gray area, width is 2σ error) is displayed. Weighted mean ages are given. The small insets show the inverse isochron diagrams.

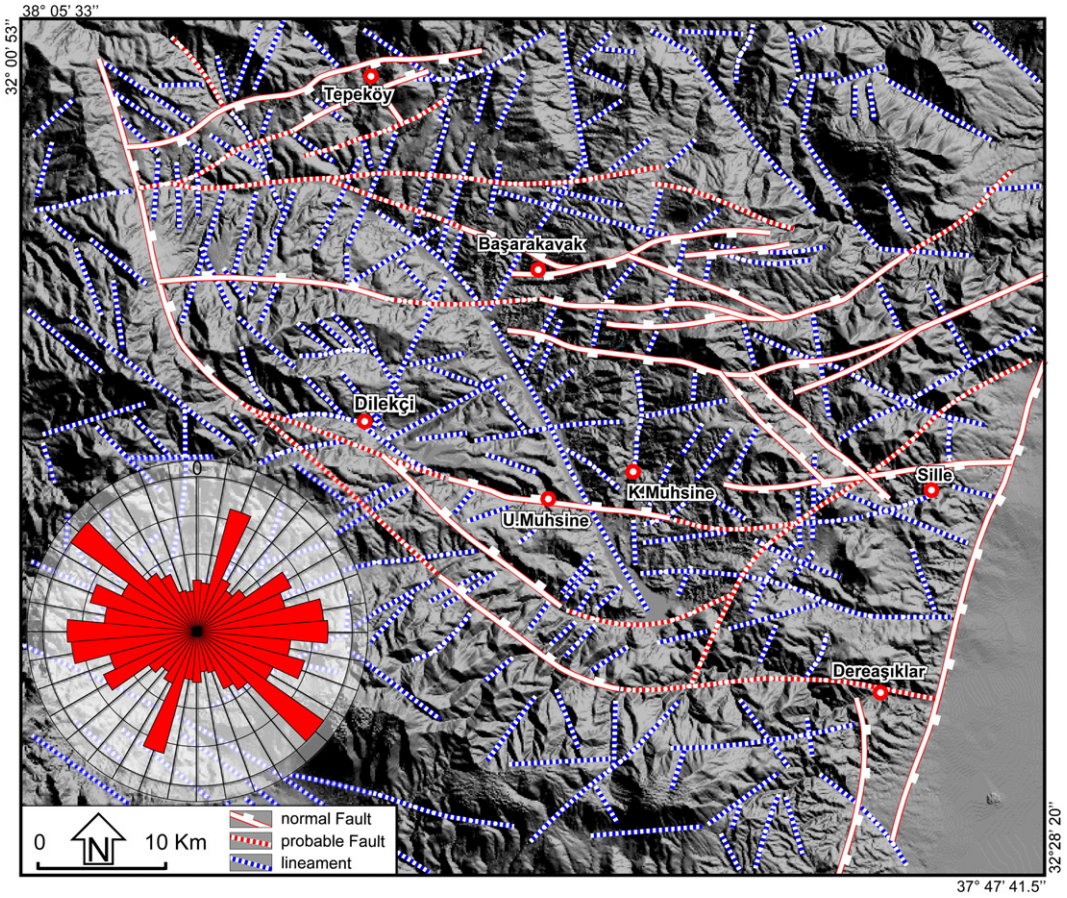

Fig. 18. Structural map of the Altınapa Basin, indicating faults and lineaments overlain on a 25 × 25m resolution digital elevation model. Rose diagram indicating orientations of both faults and lineaments.

stress on each fault plane. Paleostress analyses determine the best-fitting reduced stress tensor based on the given fault slip data, identifying the orientations of the three principal stress axes (σ_1: maximum, σ_2: intermediate and σ_3: minimum) and the shape ratio of stress ellipsoid, $\Phi = (\sigma_2 - \sigma_3)/(\sigma_1 - \sigma_3)$ ranging between two extreme values of 0 and 1. The Φ ratio constraints all-possible cases between uniaxial ($\sigma 2 = \sigma 3$; $\Phi = 0$ or $\sigma 1 = \sigma 2$; $\Phi = 1$) to tri-axial stress configurations ($\sigma 1 > \sigma 2 > \sigma 3$; $\Phi = 0.5$) (Angelier, 1994).

From 29 sites, 377 fault-slip measurements (Fig. 21a), including direction and sense of relative movements were collected. Most of the data were collected from the infill of the Altınapa Basin, and from faults juxtaposing basement and basin-fill units. Strikes of the mezoscopic fault planes clustering around E–W and NE–SW directions (Fig. 21b) are consistent with the general trend of the major faults. Dips range between 45° and 90°. Inversion of the data was carried out on each site separately and 29 stress configurations are constructed (Fig. 21c and Table 2).

5.2. Spatial characteristics

In order to understand the type of deformation, the constructed paleostress orientations are analyzed for their regional consistency. Fig. 22 shows that $\sigma 1$ is generally oriented (sub-) vertically in all sites, whereas σ_2 and σ_3 do not show a consistent direction. Such distributions are characteristic for uniaxial stress conditions and result in stress permutation in regions where the magnitudes of σ_2 and $\sigma 3$ are close to or equal to each other (Homberg et al., 1997). The deformation that affected the Altınapa Basin is clearly extensional, as indicated by the vertical σ_1, and consistent with normal fault activity along the major faults in the basin. The near equal σ_2 and σ_3 magnitudes should produce Φ values approaching zero in the case of σ_1 magnitudes much greater than that of σ_2. As seen in Fig. 22d and Table 2, the frequency distribution of Φ values are bimodal and has peak values at 0.15 and 0.35. In other words, in more than 20 sites Φ values are less than 0.5. This indicates that uniaxial stress conditions prevailed in the region.

In order to verify the compatibility of the constructed paleostress configurations relative to regional structures, the horizontal component of the minor principal stress is plotted on the map of Fig. 23. Apart from some strike-slip solutions (sites 4, 8, 15 and 19), most of the $\sigma 3$ directions are (near-) orthogonal to the dominant trends of the major structures (except for sites 3 and 6). This pattern implies unconstrained slip (somewhat similar to free fall of hanging-wall blocks along fault planes) along the major normal faults, as expected in uniaxial stress conditions. The sites with strike-slip solutions are indications of transfer faults and/or stress perturbations due to accommodation of local space problems.

5.3. Temporal relationships

In addition to spatial distribution of the paleostress directions, temporal changes of the paleostress configurations throughout the stratigraphy are very important to unravel any paleostress stratigraphy of the basin. In paleostress stratigraphy, the basement rocks potentially record the entire paleostress history during basin subsidence, whereas basin strata record paleostress tensors that were coeval with sedimentation. Structures developed in the upper most basin fill offer insight into only the youngest tectonism (Kleinspehn et al., 1989). Therefore, the younger events need to be extracted from the older ones, successively from younger to older. We therefore ordered

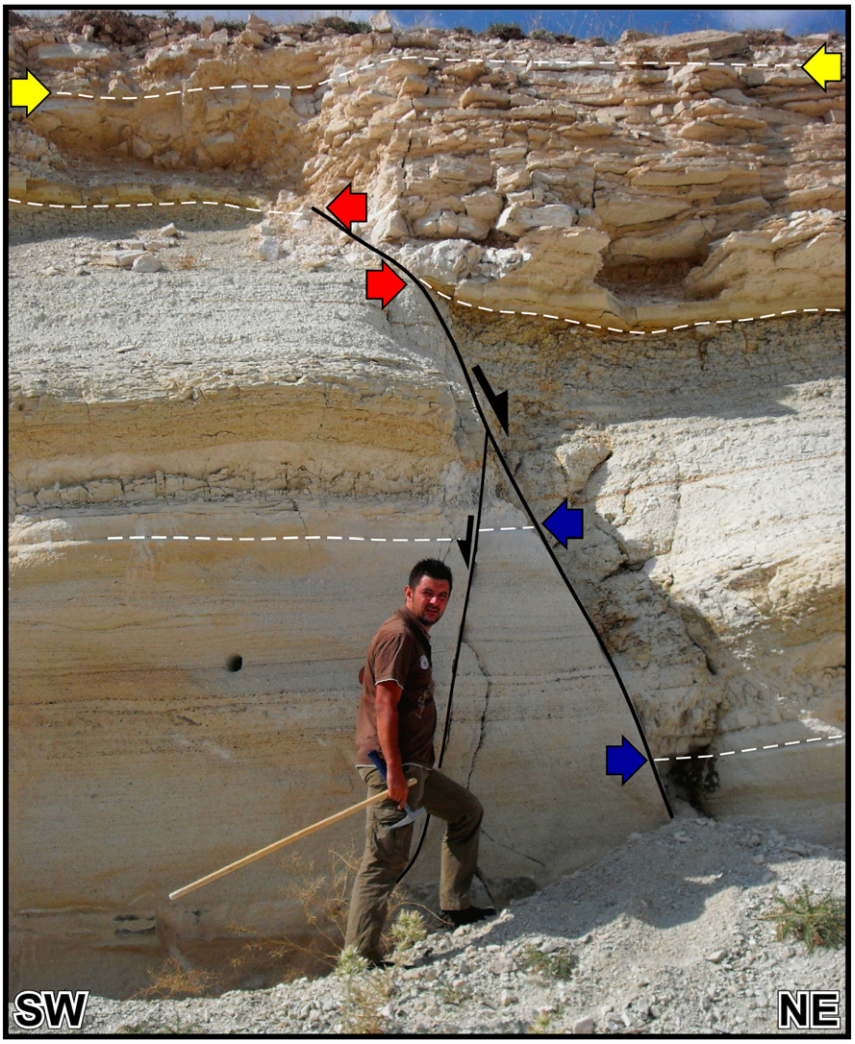

Fig. 19. Syn-sedimentary normal fault in the tuff units of Upper Altınapa Group.

our paleostress data according to the age of the rocks from which they were collected (Fig. 24), and according to cross-cutting relationships. The paleostress directions for the Lower and Upper Altınapa groups were plotted separately, and the resultant contour diagrams were compared. As seen in Figs. 22, 23 and 26, there is no notable difference between the measurements from the Lower and Upper Altınapa groups.

The youngest, still active extension direction in the Altınapa Basin is reflected by the Konya Fault, reflected by paleostress sites 10 and 15. This extension direction trends approximately E–W to NW–SE. This youngest tectonic regime is consistent with focal mechanism solutions of the Sille Earthquake (11 September 2009, Mw = 4.9, ETHZ) (Fig. 24). However, recent earthquakes along the Akşehir-Afyon Graben (AAG) to the north of the Altınapa Basin (Ergin et al., 2009; Taymaz et al., 2004) demonstrate extension directions ranging from N–S to NE–SW (Fig. 24), attesting to the fact that currently central Turkey has strongly varying σ_3 directions while σ_1 is (sub-) vertical. This is consistent with the paleostress patterns obtained throughout the stratigraphical successions of the Altınapa Basin.

6. Discussion

6.1. Altınapa Basin evolution

The Altınapa Basin developed unconformably on top of the Taurides fold-thrust belt which itself formed during subduction and collision in late Cretaceous to perhaps Oligocene time. The onset of sedimentation in the basin predates 11.8 Ma, which is the oldest age we obtained from the UAG. The age of the onset of sedimentation remains unknown, but if sedimentation rates in the LAG were comparable to those in the UAG, the onset of sedimentation may also be of Middle Miocene age. However, UAG and LAG are divided by angular unconformity with an unknown stratigraphic hiatus, which means that LAG may also be older.

Subsidence was most likely related to extension, with a N–S to NE–SW dominant direction. The fining upwards sequence in the LAG, together with the unconformable contact with the overlying lacustrine UAG suggests that most of the accommodation space was formed during UAG deposition. The dominance of coarse clastic sedimentation along the southwestern fault-controlled margin, together with the onlap of the UAG over the northeastern basin margin suggests that initial subsidence was fault (NW–SE) controlled, and that this faulting gave rise to the development of a half-graben geometry to the basin.

The E–W trending open folds that affect the LAG more than the UAG are probably extension related since no compressional faults were observed in the basin. Similarly, all of the paleostress configurations indicate extension in the basin throughout its stratigraphy since Middle Miocene. The angular unconformity observed between the LAG and UAG indicates that some erosion occurred prior to UAG deposition. This angular unconformity may mark lake level fall or complete drought possibly due to climatic

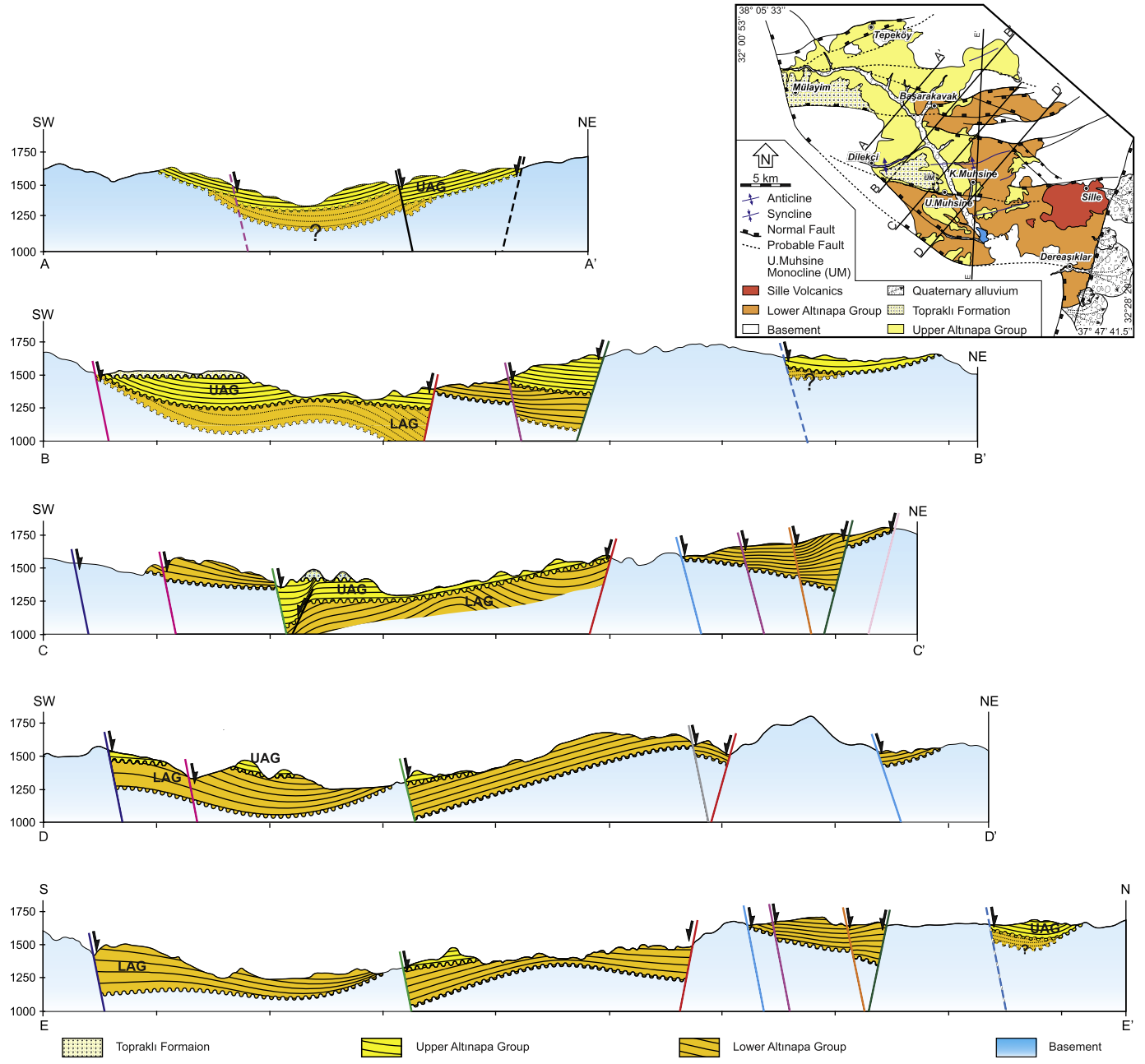

Fig. 20. Structural Cross-sections constructed from the geological map. Inset map shows the locations of the sections. Different colors for faults correspond to the same fault in different sections.

changes. Alternatively, the inception of volcanism in the vicinity of the Altınapa Basin may have led to local uplift and tilting of the LAG units. It seems unlikely that uplift was related to a local enhancement of relief, as the UAG is characterized by lacustrine deposition, and is fine-grained in nature. Our data show that since the Middle Miocene, the Altınapa Basin has been in a uniaxial extensional regime which is evidenced by spatially and temporally unconstrained extensional directions (Fig. 24).

6.2. Regional implications

Our structural and geochronological analysis of the Altınapa Basin provides evidence that extension to the north of the Tauride mountain range was already active since Middle Miocene time, and formed intramontane, continental basins on top of the late Cretaceous to Oligocene Taurides fold–thrust belt. To the south, west and southeast of the study area, sedimentation and extension in the Adana, Mut and Manavgat basins appear to have started earlier, in the Early Miocene or locally perhaps in Late Oligocene time, and was marine in character (e.g. Burton-Ferguson et al., 2005; Çiner et al., 2008; Şafak et al., 2005). Our results may indicate that inception of Neogene extension started later in the north than in the south, consistent with the diachronous onset of sedimentation younging northwards from Cyprus (Bassant et al., 2005).

Miocene extension appears to be spatially restricted to the region north of the Cyprus subduction zone. To the east of the Adana Basin (Fig. 1), Middle Miocene and younger deformation has been dominated by N–S compression and strike-slip faulting related to westward Anatolian escape as a result of the Arabia–Europe collision (e.g., Faccenna et al., 2006; Hüsing et al., 2009; Kaymakci et al., 2010; Şengör et al., 2003), and to the west of the central Taurides, Middle–Late Miocene deformation was transpressional, related to vertical axis rotations of the Bey Dağları platform and Lycian Nappes at the eastern limit of the Aegean–west Anatolian orocline (Kissel and

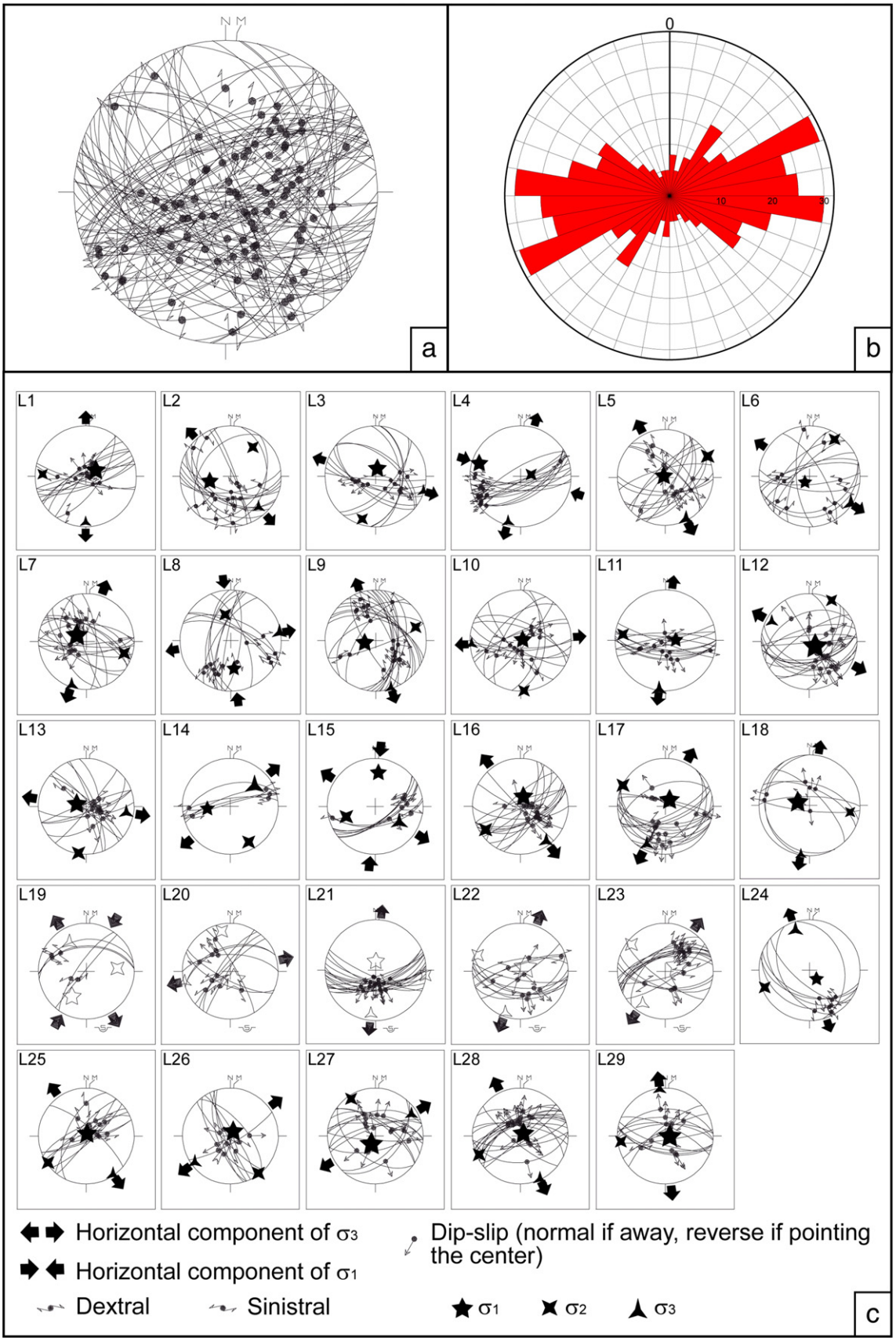

Fig. 21. (a) Stereoplot showing all of the collected fault slip measurements (N = 377), (b) bidirectional rose diagram of fault strikes. Note that there are three distinct dominant directions. (c) Stereoplots showing constructed paleostress orientations, fault planes and slip lineations (lower hemisphere equal area projection).

Table 2
Locations and paleostress orientations for whole data.

Loc	Long	Lat	σ_1(P°/D°)	σ_2(P°/D°)	σ_3(P°/D°)	Φ	Mean ANG	Mean RUP	N
L1	32.16011	38.06960	71°/059°	16°/273°	10°/180°	0.112	37	73	13
L2	32.16214	38.06511	55°/257°	28°/037°	19°/138°	0.462	28	64	15
L3	32.10005	38.01244	77°/013°	13°/197°	01°/107°	0.276	18	42	13
L4	32.20648	37.95920	12°/287°	77°/081°	05°/195°	0.360	9	24	16
L5	32.31572	37.88673	87°/318°	01°/063°	03°/153°	0.449	18	46	15
L6	32.22815	37.98963	80°/226°	10°/033°	02°/123°	0.607	25	55	12
L7	32.25550	38.03066	71°/303°	18°/107°	05°/199°	0.142	22	46	16
L8	32.25891	38.03231	44°/173°	46°/348°	03°/081°	0.597	18	33	13
L9	32.40211	37.93452	73°/259°	17°/072°	02°/162°	0.330	25	49	20
L10	32.42253	37.87497	87°/066°	01°/176°	03°/266°	0.105	23	59	15
L11	32.38741	37.85167	74°/088°	16°/278°	03°/187°	0.513	25	59	14
L12	32.42282	37.87736	77°/128°	02°/029°	13°/298°	0.094	21	44	19
L13	32.39163	37.90838	74°/284°	02°/189°	16°/099°	0.330	25	51	12
L14	32.40954	37.85433	50°/265°	18°/152°	34°/050°	0.711	45	86	5
L15	32.42488	37.88497	30°/005°	36°/250°	39°/123°	0.734	33	55	8
L16	32.35526	37.95844	73°/017°	14°/236°	10°/143°	0.311	15	37	17
L17	32.33364	37.90951	77°/034°	02°/296°	13°/206°	0.352	16	47	16
L18	32.39194	37.85823	70°/285°	20°/099°	02°/190°	0.027	11	40	7
L19	32.42945	37.99422	39°/209°	35°/085°	31°/329°	0.462	30	62	5
L20	32.38742	37.89012	74°/157°	16°/348°	03°/257°	0.176	25	56	10
L21	32.34830	37.95438	76°/002°	01°/096°	14°/186°	0.264	11	22	18
L22	32.29146	37.89938	79°/053°	06°/291°	09°/200°	0.163	21	47	11
L23	32.28899	37.97180	68°/067°	11°/308°	19°/215°	0.206	13	39	16
L24	32.34778	37.96698	72°/141°	06°/249°	17°/341°	0.580	11	29	7
L25	32.28488	37.93799	86°/019°	03°/235°	03°/145°	0.396	28	69	10
L26	32.26213	38.00526	81°/033°	03°/143°	08°/233°	0.368	30	53	9
L27	32.27441	38.00479	75°/205°	08°/327°	13°/059°	0.192	15	39	14
L28	32.24566	37.92514	83°/053°	07°/246°	01°/155°	0.307	13	42	19
L29	32.34543	37.95603	82°/096°	07°/263°	02°/353°	0.136	16	47	12

σ_1, σ_2, σ_3 magnitude ratios of principle stresses; D/P, direction/plunge; Φ stress ratio; ANG, maximum allowed angular divergence RUP, maximum allowed quality value N, number of measurement for each site.

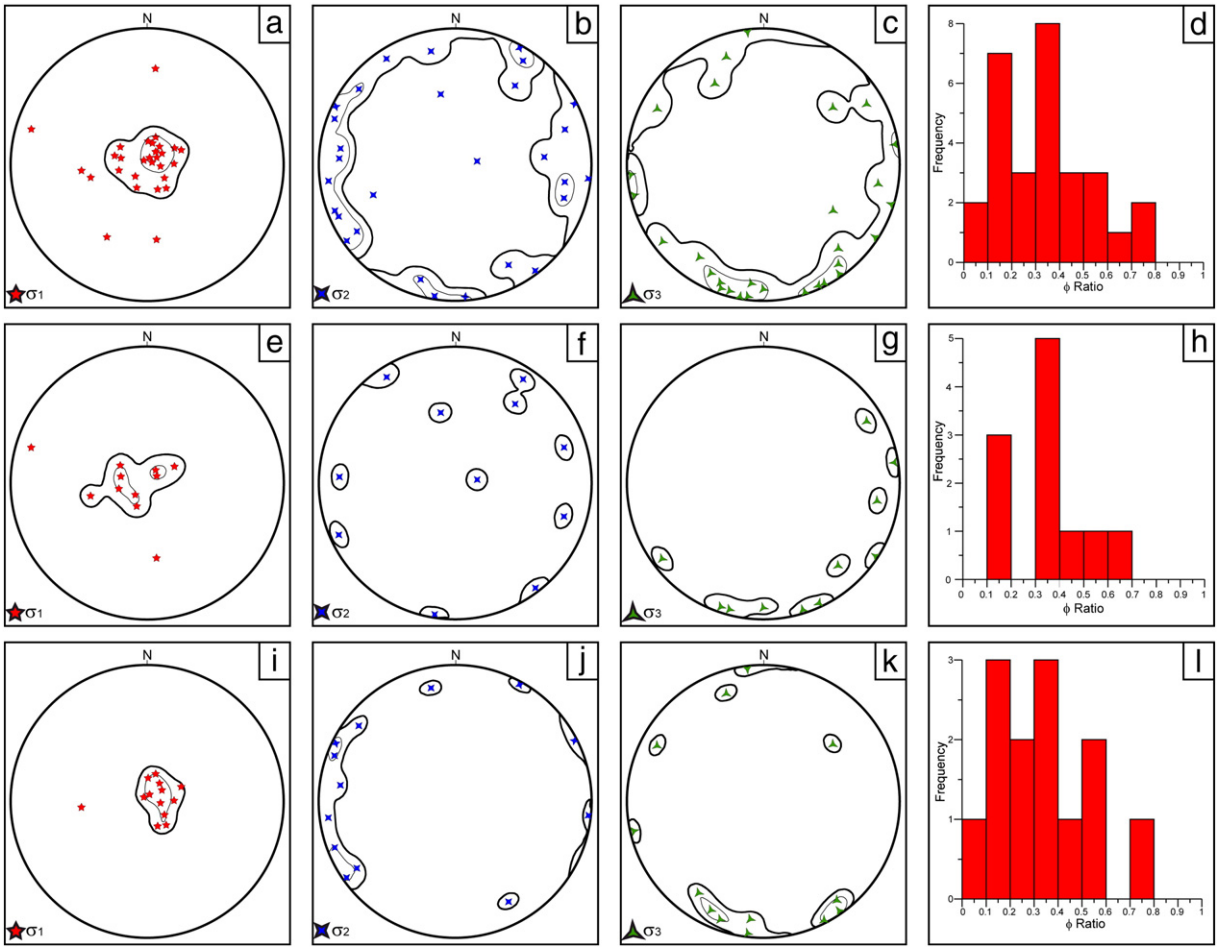

Fig. 22. Density diagrams for principal stress orientations and frequency distributions of Φ values. a–d) whole data, e–h) based on data from upper Altınapa Group, i–l) based on Lower Altınapa Group. Notice that the σ_1 is dominantly subvertical while σ_2 and σ_3 orientations are subhorizontal, with strongly varying directions indicating uniaxial stress conditions.

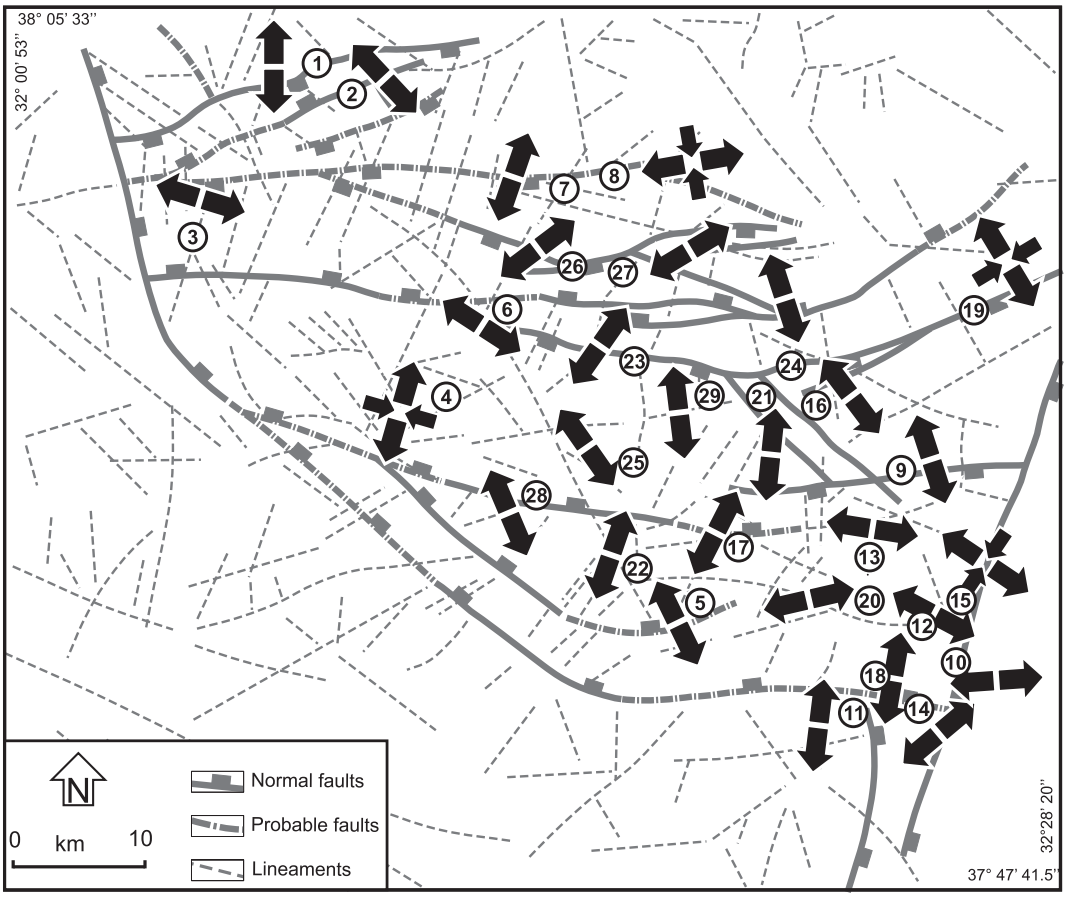

Fig. 23. (a) Major faults and lineament map of the study area. Arrows indicate horizontal component of the minor principal stress (σ_3) and numbers indicate the paleostress measurement sites which correspond to site numbers in Fig. 21c.

Poisson, 1987; Morris and Robertson, 1993; Poisson et al., 2003; van Hinsbergen, 2010; van Hinsbergen et al., 2010a,b). The spatial restriction of NE–SW to NW–SE extension to the region north of the Cyprus subduction zone suggests a direct relationship to the dynamics of the eastern Mediterranean subduction system, which has likely been in a state of relative southward trench retreat since at least Middle Miocene time (see also Over et al., 2004). Our analysis shows that not only the forearc, but also the volcanic arc region of the Cyprus subduction zone, to which the Altınapa Basin belongs, has been affected by this extension for at least the last ~12 Ma.

Finally, our analysis has an important implication for the evolution of southern Anatolian topography. In Middle to Late Miocene time, the Mut Basin, which has been uplifted since Late Miocene time to elevations up to 2 km, was marine (Cosentino et al., 2012), whereas the Altınapa Basin, currently at elevations around 1 km, was continental. No data are available to constrain the paleo-elevation of the Altınapa Basin during Middle Miocene sedimentation, but the fact that the Mut Basin lies presently at an about 1 km higher elevation than the Altınapa Basin demonstrates that the late Neogene history of the southern Turkey was characterized by strong differential uplift, with the southern Tauride mountain range uplifting at least 1 km more than the intramontane basins to their north. Cosentino et al. (2012) interpreted the uplift of the Taurides since the Late Miocene as a dynamic topographic effect, uplifting all of the Central Anatolian plateau. Although such dynamic topographic effects may have well played an important role, the major uplift difference between the Altınapa and Mut basins illustrates that at least half of the uplift of the southern Taurides resulted from regional tectonics rather than Anatolia-wide dynamic topography. The Tauride range as exposed today therefore likely represents a horst system, with regions to the north and south showing smaller magnitudes of uplift than the range itself. We finally note that the modern topography of the Tauride range is thus a late Neogene phenomenon that is unrelated to the late Cretaceous to Oligocene folding and thrusting responsible for the dominant deformation within the range.

7. Conclusions

Our results demonstrate that the Altınapa Basin is an extensional basin, with a stratigraphy that can be subdivided in a Lower and Upper Altınapa Group. Volcanic deposits in the Upper Altınapa Group have been dated with $^{40}Ar/^{39}Ar$ geochronology, and demonstrate an age range of ~11.8–11.6 Ma. Extension-related subsidence, controlled along large basin-bounding faults, therefore started prior to 11.8 Ma. Paleostress analysis shows that σ_2 and σ_3 directions during and after deposition, up to and including the modern-day patterns, vary strongly and locally. A regional pattern of open, extension-related folds shows an approximately E–W trend and suggests that the dominant extension direction responsible for formation of the basin was ~N–S to NE–SW. These folds affect the Lower Altınapa Group more than the Upper Altınapa Group, between which an angular unconformity exists. This, together with the fact that the Lower Altınapa Group has a clear fining upward trend, suggests that the main basin forming phase predates 11.8 Ma. Our results are consistent with a regional pattern of NE–SW to NW–SE extension along the southern Taurides, which seems spatially coincident with the location of the Cyprus subduction zone.

The continental Middle Miocene sediments of the Altınapa Basin lie at present at an elevation of ~1 km, whereas partly contemporaneous marine deposits in the Mut Basin to the south, on top of the Tauride range, are elevated up to 2 km. This demonstrates that the southern

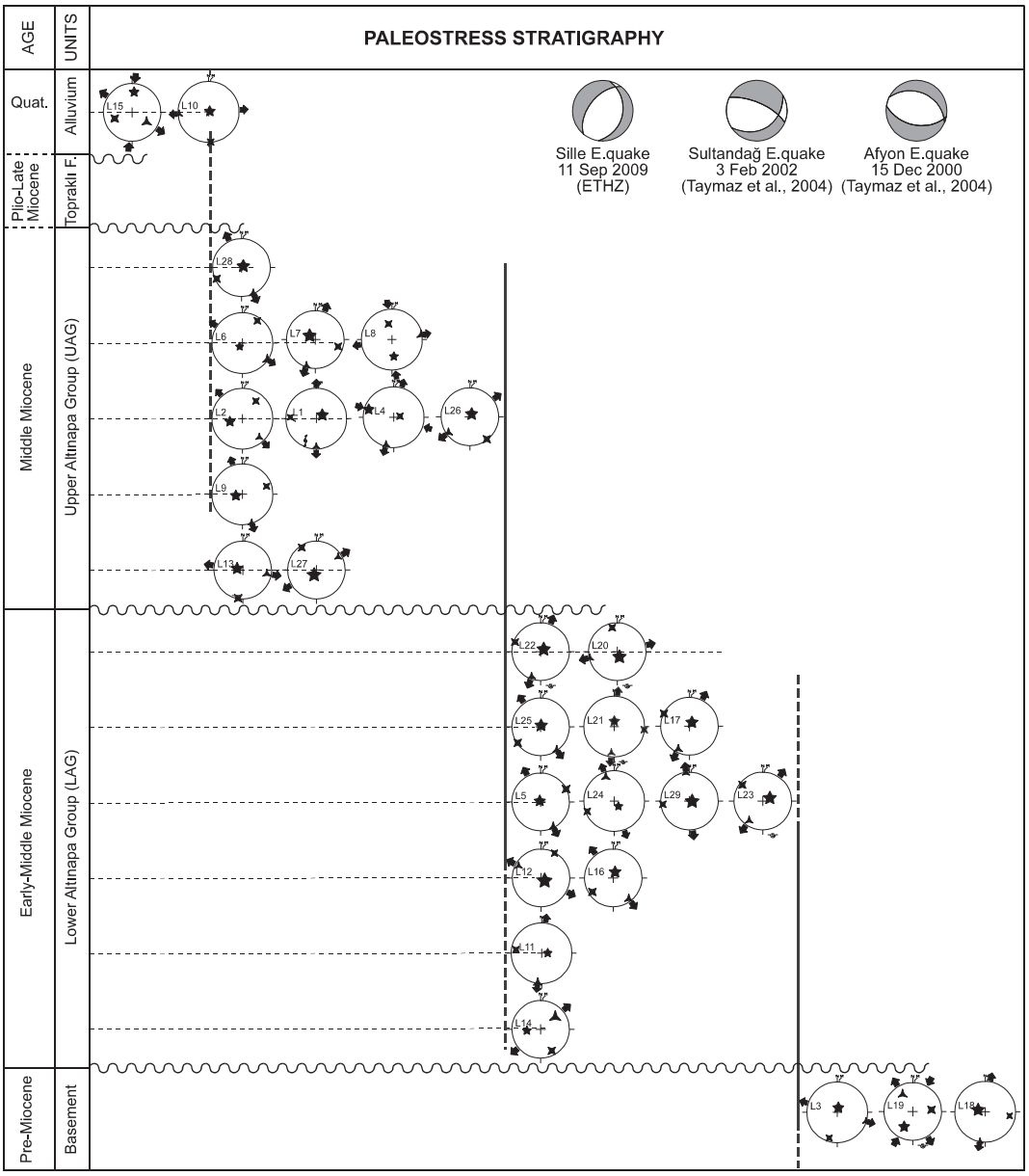

Fig. 24. Paleostress stratigraphy of the Apa Basin from the Middle Miocene to Recent. Arrows represent σ_3 directions. 1) 11 September 2009 Sille Earthquake (Mw = 4.9, ETHZ), 2) 15 December 2000 Afyon Earthquake (Ms = 5.8, Taymaz et al., 2004), 3), 03 February 2002 Sultandağı Earthquake (Ms = 6.4, Taymaz et al., 2004). Note that the unconstrained nature of σ_3 directions and from Middle Miocene to Recent and variation of extension directions of recent earthquakes in the region.

Tauride range uplifted at least 1 km more than the flanking intramontane basins to the north, attesting to strong differential uplift in the late Neogene of southern Turkey. The high topography of the Tauride range is unrelated to the late Cretaceous to Oligocene thrusting that deformed the rocks in the range.

Acknowledgments

Research for this paper occurred within the context of the Netherlands Research School of Integrated Solid Earth Sciences (ISES) and was supported by ÖYP research fund of Turkish Government No: BAP-08-11-DPT.2002K120510 and DARIUS Programme. DJJvH acknowledges financial support from Statoil (SPlates Model project). KK is funded by grant 814.01.004 of the Netherlands Organisation for Scientific Research. AK would like to thank Kemal Koç, Hasan Kocatepe, M. Onur Öztepe, Erhan Gülyüz, Murat Özkaptan, Mustafa Y. Kaya, Kıvanç Yücel and Şule Gürboğa for their support during fieldworks in 2008 and 2009. Finally, we thank Domenico Cosentino and an anonymous reviewer for their valuable comments.

Appendix A. Supplementary data

Supplementary data to this article can be found online at doi:10.1016/j.tecto.2012.01.028.

References

Alçiçek, H., 2010. Stratigraphic correlation of the Neogene basins in southwestern Anatolia: regional palaeogeographical, palaeoclimatic and tectonic implications. Palaeogeography, Palaeoclimatology, Palaeoecology 291, 297–318.

Altıner, D., Yılmaz, I.O., Ozgul, N., Akcar, N., Bayazıtoglu, M., Gaziulusoy, Z.E., 1999. High-resolution sequence stratigraphic correlation in the Upper Jurassic (Kimmeridgian)–Upper Cretaceous (Cenomanian) peritidal carbonate deposits (Western Taurides, Turkey). Geological Journal 34, 139–158.

Andrew, T., Robertson, A.H.F., 2002. The Beysehir–Hoyran–Hadim nappes: genesis and emplacement of Mesozoic marginal and oceanic units of the northern Neotethys in southern Turkey. Journal of the Geological Society of London 159, 529–543.
Angelier, J., 1990. Inversion of field data in fault tectonics to obtain the regional stress—III. A new rapid direct inversion method by analytical means. Geophysical Journal International 103, 363–376.
Angelier, J., 1994. Fault slip analysis and paleostress reconstruction. In: Hancock, P.L. (Ed.), Continental Deformation. Pergamon Press, Oxford, pp. 53–101.
Barrier, E., Vrielynck, B., 2008. MEBE Atlas of Paleotectonic maps of the Middle East. Commission for the Geological Map of the World. .
Bassant, P., van Buchem, F.S.P., Strasser, A., Görür, N., 2005. The stratigraphic architecture and evolution of the Burdigalian carbonate–siliciclastic sedimentary systems of the Mut Basin, Turkey. Sedimentary Geology 173, 187–232.
Besang, C., Eckhart, F.J., Harre, W., Kreuzer, G., Muller, P., 1977. Radiometrische Alterbestimmung am neogenen Eruptivgesteinen der Türkei. Geologisches Jahrbuch 25, 3–36.
Biryol, C.B., Beck, S.L., Zandt, G., Ozacar, A.A., 2011. Segmented African lithosphere beneath the Anatolian region inferred from teleseismic P-wave tomography. Geophysical Journal International 184, 1037–1057.
Blumenthal, M.M., 1963. Le système structural du Taurus sud Anatolies. Bull. Soc. Géol. Fr. Livre à Mémoire de Professor P. Fallot, Mémoir hors-série, 1, pp. 611–662.
Burton-Ferguson, R., Aksu, A.E., Calon, T.J., Hall, J., 2005. Seismic stratigraphy and structural evolution of the Adana Basin, eastern Mediterranean. Marine Geology 221, 189–222.
Carey, E., Burinier, B., 1974. Analyse théorique et numérique d'un modèle mécanique élémentaire appliqué à l'étude d'une population de failes. Comptes Rendus de l' Academie des Sciences Paris D279, 891–894.
Çiner, A., Karabiyikoglu, M., Monod, O., Deynoux, M., Tuzcu, S., 2008. Late Cenozoic sedimentary evolution of the Antalya Basin, Southern Turkey. Turkish Journal of Earth Sciences 17, 1–41.
Cosentino, D., Schildgen, T.F., Cipollari, P., Faranda, C., Gliozzi, E., Hudácková, N., Lucifora, S., Strecker, M.R., 2012. Late Miocene surface uplift of the southern margin of the Central Anatolian Plateau, Central Taurides, Turkey. Geological Society of America Bulletin 124 (1–2), 133–145. doi:10.1130/B30466.1.
Darbas, G., Nazik, A., 2010. Micropaleontology and paleoecology of the Neogene sediments in the Adana Basin (South of Turkey). Journal of Asian Earth Sciences 39, 136–147.
Derman, A.S., Gürbüz, K., 2007. Nature, provenance and relationships of Early Miocene palaeovalley fills, northern Adana Basin, Turkey: their significance for sediment-bypassing on a carbonate shelf. Turkish Journal of Earth Sciences 16, 181–209.
Doğan, A., 1975. Sizma–Ladik (Konya) Civa Sahasinin Jeolojisi ve Maden Yataklari Sorunlarinin Incelenmesi. I.Ü. Fen Fakültesi Min. Pet. Kürsüsü, Yük. Müh. Diploma Çalismasi, Istanbul., 40.
Eren, Y., 1992. Eldes-Gökçeyurt-Derbent (Konya kuzeybatisi) Dolaylarinda Kocaçaldağ Yükseltisinin Jeolojisi. S.Ü. Arastirma Fonu, Proje No: 88-026. .
Eren, Y., 1993. Eldes-Derbent-Tepeköy-Sögütözü Arasinin Jeolojisi, PhD Thesis, S.Ü. Fen Bil. Enst. Konya, Turkey. 224.
Eren, Y., 1996. Ilgin-Sarayönü (Konya) güneyinde Bozdaglar Masifinin Yapisal Özellikleri. Geological Bulletin of Turkey 39, 49–64.
Ergin, M., Aktar, M., Özalaybey, S., Tapirdamaz, M.C., Selvi, O., Tarancioglu, A., 2009. A high-resolution aftershock seismicity image of the 2002 Sultandagi-Çay earthquake (Mw—6.2), Turkey. Journal of Seismology 13, 633–646.
Eriş, K.K., Bassant, P., Ülgen, U.B., 2005. Tectono-stratigraphic evolution of an Early Miocene incised valley-fill (Derinçay Formation) in the Mut Basin, Southern Turkey. Sedimentary Geology 173, 151–185.
Etchecopar, A., Vasseur, D., Daignières, M., 1981. An inverse problem in microtectonics for determination of stress tensors from faults striation analysis. Journal of Structural Geology 3, 51–65.
Faccenna, C., Bellier, O., Martinod, J., Piromallo, C., Regard, V., 2006. Slab detachment beneath eastern Anatolia: a possible cause for the formation of the North Anatolian Fault. Earth and Planetary Science Letters 242, 85–97.
Gans, C.R., Beck, S.L., Zandt, G., Biryol, C.B., Ozacar, A.A., 2009. Detecting the limit of slab break-off in central Turkey: new high-resolution Pn tomography results. Geophysical Journal International 179, 1566–1572.
Göğer, E., Kıral, K., 1969. Kizilören Dolayinin Jeolojisi. M.T.A. Rappor, 5204.
Görmüş, M., 1984. Kizilören (Konya), Dolayinin Jeoloji Incelemesi. S. Ü. Fen Bil. Enst. M. Sc, Konya, Turkey, 67.
Gül, M., 2007. Effects of antecedent topography on reefal carbonate deposition: Early–Middle Miocene of the Adana Basin, S Turkey. Journal of Asian Earth Sciences 31, 18–34.
Homberg, C., Hu, J.-C., Angelier, J., Bergerat, F., Lacombe, O., 1997. Characterization of stress perturbations near major fault zones : insights from field studies (Jura Mountains) and numerical modelling. Journal of Structural Geology 19, 703–718.
Hüsing, S.K., Zachariasse, W.J., van Hinsbergen, D.J.J., Krijgsman, W., Inceöz, M., Harzhauser, M., Mandic, O., Kroh, A., 2009. Oligo-Miocene foreland basin evolution in SE Anatolia: constraints on the closure of the eastern Tethys gateway. In: van Hinsbergen, D.J.J., Edwards, M.A., Govers, R. (Eds.), Collision and Collapse at the Africa-Arabia-Eurasia subduction zone: Geological Society, London, Special Publication, pp. 107–132.
Janson, X., van Buchem, F.S.P., Dromart, G., Eichenseer, H.T., Dellamonics, X., Boichard, R., Bonnaffe, F., Eberli, G.P., 2010. Architecture and facies differentiation within a Middle Miocene carbonate platform, Ermenek, Mut Basin, southern Turkey. In: van Buchem, F.S.P., Gerdes, K.D., Esteban, M. (Eds.), Mesozoic and Cenozoic Carbonate Systems of the Mediterranean and the Middle East: Stratigraphic and Diagenetic Reference Models: Geological Society, London, Special Publications, pp. 265–290.
Karabıyıkoğlu, M., Tuzcu, S., Çiner, A., Deynoux, M., Örçen, S., Hakyemez, A., 2005. Facies and environmental setting of the Miocene coral reefs in the late-orogenic fill of the Antalya Basin, western Taurides, Turkey: implications for tectonic control and sea-level changes. Sedimentary Geology 173, 345–371.
Altiekin (Konya) civarinin jeolojisi ve mineralojik-petrografik incelenmesi. MSc thesis, Selçuk University, Konya.
Kaymakci, N., Özçelik, Y., White, S.H., van Dijk, P.M., 2009. Tectono-stratigraphy of the Çankiri Basin: late Cretaceous to early Miocene evolution of the Neotethyan suture zone in Turkey. In: van Hinsbergen, D.J.J., Edwards, M.A., Govers, R. (Eds.), Collision and Collapse at the Africa-Arabia-Eurasia subduction zone: Geological Society of London Special Publication, pp. 67–106.
Kaymakci, N., Inceöz, M., Ertepinar, P., Koç, A., 2010. Late Cretaceous to Recent kinematics of SE Anatolia (Turkey). In: Sosson, M., Kaymakci, N., Stephenson, R.A., Bergerat, F., Starostenko, V. (Eds.), Sedimentary basin tectonics from the Black Sea and Caucasus to the Arabian Platform: Geological Society, London, Special Publications, pp. 409–435.
Keller, J., Jung, D., Burgath, K., Wolff, F., 1977. Geologie und Petrologie des Neogenen Kalkalkalivulkanismus von Konya (Erenler Dagi, Alacadag Massiv, Zentral Anatolian). Geologisches Jahrbuch, B 25, 37–117.
Keskin, M., 2003. Magma generation by slab steepening and breakoff beneath a subduction–accretion complex: an alternative model for collision-related volcanism in Eastern Anatolia, Turkey. Geophysical Research Letters 30 (24), 8046. doi:10.1029/2003GL018019.
Khair, K., Tsokas, G.N., 1999. Nature of the Levantine (eastern Mediterranean) crust from multiple-source Werner deconvolution of Bouguer gravity anomalies. Journal of Geophysical Research 104, 25469–25478.
Kissel, C., Poisson, A., 1987. Étude paléomagnetique préliminaire des formations cénozoïques des Bey Daglari (Taurides occidentales, Turquie). Comptes Rendus de l' Academie des Sciences Paris 304 (8), 343–348 Série II.
Kleinspehn, K.L., Pershing, J.C., Teyssier, C., 1989. Paleostress stratigraphy: a new technique for analyzing tectonic control on sedimentary-basin subsidence. Geology 17, 253–256.
Koppers, A.A.P., 2002. ArArCALC-software for $^{40}Ar/^{39}Ar$ age calculations. Computers & Geosciences 28, 605–619.
Kuiper, K.F., Deino, A.L., Hilgen, F.J., Krijgsman, W., Renne, P.R., Wijbrans, J.R., 2008. Synchronizing rock clocks of Earth history. Science 320, 500–504.
Mackintosh, P., Robertson, A.H.F., 2009. Structural and sedimentary evidence from the northern margin of the Tauride platform in south central Turkey used to test alternative models of Tethys during Early Mesozoic time. Tectonophysics 473, 149–172.
Meijers, M.J.M., Kaymakci, N., van Hinsbergen, D.J.J., Langereis, C.G., Stephenson, R.A., Hippolyte, J.-C., 2010. Late Cretaceous to Paleocene oroclinal bending in the Central Pontides (Turkey). Tectonics 29, TC4016. doi:10.1029/2009TC002620.
Meijers, M.J.M., van Hinsbergen, D.J.J., Dekkers, M.J., Altiner, D., Kaymakci, N., Langereis, C.G., Stephenson, R.A., 2011. Pervasive Paleogene remagnetization of the central Taurides fold-and-thrust belt (southern Turkey) and implications for rotations in the Isparta Angle. Geophysical Journal International 184, 1090–1112.
Min, K., Mundil, R., Renne, P.R., Ludwig, K.R., 2000. A test for systematic errors in 40Ar/39Ar geochronology through comparison with U/Pb analysis of a 1.1-Ga rhyolite. Geochimica et Cosmochimica Acta 64, 73–98.
Morgan, L.E., Renne, P.R., Taylor, R.E., WoldeGabriel, G., 2009. Archaeological age constraints from extrusion ages of obsidian: examples from the Middle Awash, Ethiopia. Quaternary Geochronology 4, 193–203.
Morris, A., Robertson, A.H.F., 1993. Miocene remagnetisation of carbonate platform and Antalya Complex units within the Isparta Angle, SW Turkey. Tectonophysics 220, 243–266.
Niehoff, W., 1961. 1/100.000 ölçekli Aksehir 90/2 paftasi, Ilgin 91/1, 91/3 ve 91/4 paftalari üzerinde 1961 yaz mevsiminde yapilmis revizyon çalismalari hakkinda rapor. M.T.A. Rappor, 3387.
Nier, A.O., 1950. A redetermination of the relative abundances of the isotopes of carbon, nitrogen, oxygen, argon, and potassium. Physical Review 77, 789.
Öğütcü, Z., Horason, G., Kalafat, D., 2010. Investigation of microseismic activity sources in Konya and its vicinity, central Turkey. Natural Hazards 58 (1), 497–509. doi:10.1007/s11069-010-9683-6.
Okay, A.I., Özgül, N., 1984. HP/LT metamorphism and the structure of the Alanya Massif, Southern Turkey: an allochthonous composite tectonic sheet. In: Dixon, J.E., Robertson, A.H.F. (Eds.), The Geological Evolution of the Eastern Mediterranean: Geological Society Special Publication, pp. 429–439.
Okay, A.I., Satir, M., Maluski, H., Siyako, M., Monié, P., Metzger, R., Akyüz, S., 1996. Paleo- and Neo-Tethyan events in northwestern Turkey: geologic and geochronologic constraints. In: Yin, A., Harrison, T.M. (Eds.), The tectonic evolution of Asia. Cambridge University Press, Cambridge, pp. 420–441.
Okay, A.I., Zattin, M., Cavazza, W., 2010. Apatite fission-track data for the Miocene Arabia–Eurasia collision. Geology 38, 35–38.
Over, S., Ozden, S., Ulugenc, U.C., 2004. Late Cenozoic stress distribution along the Misis Range in the Anatolian, Arabian, and African plate intersection region, SE Turkey. Tectonics 23, TC3008. doi:10.1029/2002TC001455.
Özcan, A., Göncüoğlu, M.C., Turhan, N., Şentürk, K., Uysal, S., Isik, A., 1990. Konya-Kadinhani-Ilgin Dolayinin Temel Jeolojisi. M.T.A. Rappor, 9535.
Özer, E., Koc, H., Ozsayar, T.Y., 2004. Stratigraphical evidence for the depression of the northern margin of the Menderes–Tauride Block (Turkey) during the Late Cretaceous. Journal of Asian Earth Sciences 22, 401–412.
Özkan, A.M., 1998. Konya Batisindaki Neojen Çökellerinin Stratigrafisi ve Sedimantolojisi, PhD Thesis, S.Ü. Fen Bil. Enst., Konya, Türkey, 208 pp.
Özkan, A.M., Söğüt, A.R., 1999. Dilekçi (Konya batısı) çevresindeki Neojen çökellrinin stratigrafisi. Journal of Engineering Science 5, 1131–1138.
Poisson, A., Wernli, R., Sagular, E.K., Temiz, H., 2003. New data concerning the age of the Aksu Thrust in the south ofthe Aksu valley, Isparta Angle (SW Turkey): consequences for the Antalya Basin and the Eastern Mediterranean. Geological Journal 38, 311–327.

Pourteau, A., Candan, O., Oberhänsli, R., 2010. High-pressure metasediments in central Turkey: constraints on the Neotethyan closure history. Tectonics 29, TC5004. doi:10.1029/2009TC002650.
Ricou, L.E., Argyriadis, I., Marcoux, J., 1975. L'axe calcaire du Taurus, un alignement de fenêtres arabo-africaines sous des nappes radiolaritiques, ophiolitiques et métamorphiques. Bulletin de la Societe Geologique de France 17, 1024–1043.
Şafak, Ü., Kelling, G., Gökçen, N.S., Gürbüz, K., 2005. The mid-Cenozoic succession and evolution of the Mut basin, southern Turkey, and its regional significance. Sedimentary Geology 173, 121–150.
Şengör, A.M.C., Yılmaz, Y., 1981. Tethyan evolution of Turkey: a plate tectonic approach. Tectonophysics 75, 181–241.
Şengör, A.M.C., Özeren, S., Genç, T., Zor, E., 2003. East Anatolian high plateau as a mantle-supported, north–south shortened domal structure. Geophysical Research Letters 30 (24), 8045. doi:10.1029/2003GL017858.
Steiger, R.H., Jäger, E., 1977. Subcommission on geochemistry: convention on the use of decay constants in geo- and cosmochronology. Earth and Planetary Science Letters 36, 359–362.
Taymaz, T., Tan, O., Yolsal, S., 2004. Seismotectonics of western Turkey: a synthesis of source parameters and rupture histories of Recent earthquakes. Eos Transactions AGU 85, 47.
Temel, A., Gündogdu, M.N., Gourgaud, A., 1998. Petrological and geochemical characteristic of Cenozoic high-K calcalkaline volcanism in Konya, Central Anatolia, Turkey. Journal of Volcanology and Geothermal Research 85, 327–354.
Torsvik, T.H., Cocks, L.R.M., 2009. The Lower Palaeozoic palaeogeographical evolution of the northeastern and eastern peri-Gondwanan margin from Turkey to New Zealand. In: Bassett, M.G. (Ed.), Early Palaeozoic Peri-Gondwana terranes: New insights from tectonics and biogeography: Geological Society, London, Special Publications, pp. 3–21.
van Hinsbergen, D.J.J., 2010. A key extensional metamorphic complex reviewed and restored: the Menderes Massif of western Turkey. Earth-Science Reviews 102, 60–76.
van Hinsbergen, D.J.J., Dekkers, M.J., Bozkurt, E., Koopman, M., 2010a. Exhumation with a twist: paleomagnetic constraints on the evolution of the Menderes metamorphic core complex (western Turkey). Tectonics 29, TC3009. doi:10.1029/2009TC002596.
van Hinsbergen, D.J.J., Dekkers, M.J., Koç, A., 2010b. Testing Miocene remagnetization of Bey Daglari: Timing and amount of Neogene rotations in SW Turkey. Turkish Journal of Earth Sciences 19, 123–156.
van Hinsbergen, D.J.J., Kaymakci, N., Spakman, W., Torsvik, T.H., 2010c. Reconciling the geological history of western Turkey with plate circuits and mantle tomography. Earth and Planetary Science Letters 297, 674–686.
Wiesner, K., 1968. Konya civa yataklari ve bunlar üzerindeki etütler. M.T.A. Dergisi, Sayi, 70, pp. 178–213.
Yağmurlu, F., 1991a. Stratigraphy and depositional environments of Yalvaç-Yarıkkaya Neogene basin, SW-Anatolia. Geological Bulletin of Turkey 34, 9–19.
Yağmurlu, F., 1991b. Yalvaç-Yarikkaya Neojen havzasinin tektono-sedimanter özellikleri ve yapisal evrimi. M.T.A. Dergisi, Sayi, 112, pp. 1–13.
Yetiş, C., 1988. Reorganization of the Tertiary stratigraphy in the Adana basin, southern Turkey. Newsletters in Stratigraphy 20, 43–58.